National Chiao Tung University

Institute of Electro-Optical Engineering

Master Thesis

Characterization techniques for fiber Bragg gratings

布拉格光纖光柵特性量測技術

Graduate Student: I-Lin Wu(吳易霖)

Adviser: Dr. Yin-Chieh Lai(賴暎杰博士)

June, 2004

Characterization techniques for fiber Bragg gratings

布拉格光纖光柵特性量測技術

Graduate Student: I-Lin Wu(吳易霖)

Advisor: Dr. Yin-Chieh Lai(賴暎杰博士)

國立交通大學

光電工程研究所

碩士論文

A Thesis

Submitted to Electro-Optical Engineering

College of Electrical Engineering and Computer Science

National Chiao-Tung University

June 2004

Hsinchu, Taiwan

公元 2004 年六月

Characterization techniques for fiber Bragg gratings

Student:I-Lin Wu Advisor:Dr. Yin-Chieh Lai

Institude of Electro-optical Engineering

College of Electrical and Computer Science

National Chiao-Tung University

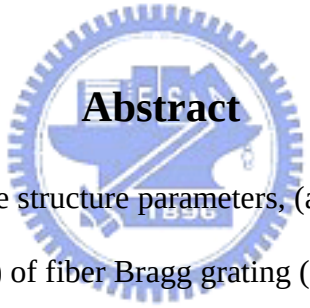

Abstract

In this thesis we measure the structure parameters, (ac index modulation profile and variation of the grating period) of fiber Bragg grating (FBG) devices by the direct side diffraction interference method. We demonstrate the accuracy of $1*10^{-6}$ for the measurement of ac index modulation and 0.01nm for the measurement of the grating period variation with a spatial resolution of 80 μm. The measured ac index profile and variation of the grating period are consistent with the intensity distribution of the UV writing laser and the chirp rate of the phase mask used in the experiment. The reflection and transmission spectra simulated by the transfer matrix method with the measured ac index and grating period are consistent with those measured by the optical spectrum analyzer. The ac index profile reconstructed from indirect “discrete Layer-Peeling method” is also consistent with that measured by the side diffraction interference method.

布拉格光纖光柵特性量測技術

研究生：吳易霖　　指導教授：賴暎杰 博士

國立交通大學光電工程研究所

電機資訊學院

摘要

在本論文中,我們使用直接側向繞射與干涉方法來量測光纖光柵的結構參數，如折射率調變變化與光柵週期之變化。在量測折射率調變的方面我們可以達到 $1*10^{-6}$ 的準確度，而在量測光柵週期方面則可達到 0.01nm 的準確度，整個量測的空間解析度是 80 μm。所量測到的折射率調變跟光柵週期變化與製作光柵時的參數與光罩規格相符,而使用轉換矩陣法跟所量得的結構參數所模擬出來的相對應光柵頻譜特性與光譜儀所量得的相吻合,同時使用間接離散剝皮法所反推出的光柵折射率調變也與直接側向繞射所量得的光柵折射率調變相同。

Special Thanks

在交大念研究所的兩年之中，一直對賴暎杰老師專業上的博學多聞感到印象深刻，老師不僅學識淵博在待人處事上更可以說是溫文有理，今天能夠順利畢業首先要感謝的就是我的指導教授賴暎杰博士。另外實驗室博士班莊凱評學長在課業跟實驗上也對我幫忙非常的多，尤其是對於實驗的實做部分學長更是助益良多。從清大換到交大的這兩年裡認識了許多新朋友慧萍、宗正、彥緒、夙鴻、坤璋、亞琪、謹綱，和她們之間課業上的討論跟日常生活的互動讓我充實的度過了碩士班生活。碩士班兩年很快就過去了，在這兩年之中對於人生又有了一些新的感受與體悟。最後我要感謝我的父母跟一些我的好朋友，謝謝妳（你）們的關心跟照顧。

Contents:

Diagram contents:

Chapter 1 Introduction

1.1 The history of fiber Bragg gratings and their characterization techniques

As the coming of the internet age, the demand for the bandwidth of the telecommunication is getting larger and larger. Optical fibers have revolutionized telecommunication. Much of the success of the optical fiber lies in its near-ideal properties: low transmission loss, high optical damage threshold, and low optical nonlinearity. The combination of these properties has enabled long distance communication to become a reality. The refractive index profile of an optical fiber is shown in Fig1.1. The core region (d≒10um) has a higher refractive index than the surrounding cladding (d≒125um) material, which is usually made of silica. Light is therefore trapped in the core by total internal reflection at the core-cladding boundaries and is able to travel tens of kilometers with little attenuation in the 1550-nm wavelength region [1]. An ultraviolet-induced optical-fiber phase grating consists of a periodic modulation of the core refractive index in a single mode fiber written by intense ultraviolet radiation [2]. Fiber gratings have a wide range of attractive applications in modern fiber optic technology. For example, they serve as narrow band reflection or transmission filters [3]-[5] or as laser components [6]. These gratings provide a basis for fiber compatible devices for all optical signal processing applications, including sensors [7], channel selection in wavelength division multiplexing networks, and compensation for chromatic dispersion [8][9]. The advantages of fiber gratings over competing technologies include their all fiber geometry, low insertion loss, high return loss or extinction, flexibility for obtaining desired spectral characteristics [10], and potential low cost. However, the increasing

complexity and more demanding specifications of fiber gratings for such diverse applications require increasingly precise measurements of the grating structure parameters for improvement of design and fabrication. The spatial quality of fiber Bragg gratings determined the performance of the FBG-based optical communication devices, such as filters and dispersion compensators. FBGs are typically characterized spectroscopically, for example, by measuring the reflectivity and phase. The spatial characteristics of gratings can be restored from the spectroscopic data only approximately, especially for strong gratings. In addition, such methods are not necessarily efficient in determining the precise nature and location of defects in the written structure. Optical low-coherence reflectometry [11][12] is an interferometric technique that has been developed to characterize the locations of weakly reflecting defects in optical waveguides, and it is well suited for obtaining this missing spatial information [13]. However in the case of strong and highly reflecting gratings the method is severely limited. A heat scanning technique [14] has been demonstrated, but it is not efficient for weak gratings.

A fiber Bragg grating is an optical fiber for which the refractive index in the core is perturbed forming a periodic or quasi-periodic index modulation profile as shown in Fig1.2. By modulating the quasi periodic index perturbation in amplitude or period or phase, we may obtain different optical filter characteristics and different applications, such as dispersion compensator, fiber sensor, fiber laser, modulator, demodulator, wavelength selector. A narrow band of incident optical field within fiber is reflected by successive, coherent scattering from the index variations, when the following phase matching condition is achieved:

$$\lambda_B = 2n_{eff}\Lambda \qquad (1.1)$$

where λ_B is the Bragg wavelength, n_{eff} is the effective modal index and Λ is the grating period. The mode coupling or the reflection is maximum at this wavelength. The phenomenon of fiber photosensitivity was first discovered by Hill el al in 1978 [3]. Hill el al used the argon ion laser to form standing wave in the germania doped silica fiber and then induced periodic variation of refractive index. This is the first developed fiber grating, but the Bragg wavelength is fixed and the efficiency is rather low. Photosensitivity means that the exposure of UV light leads to a rise in the refractive index of certain doped glasses. Typical values for the index change are ranging between 10^{-6} to 10^{-3}, depending on the UV-exposure and the dopants in the fiber. By using the techniques like hydrogen loading [15], an index change as high as 10^{-2} can be achieved. Fiber gratings are nowadays usually fabricated by a variant of the transverse holographic methods first proposed by Meltz et al [6]. By exposing the fiber to the UV interference pattern from the side, the pattern is printed into the fiber, as shown in Fig1.3. Only the core is usually doped (for example with germanium), and consequently the grating is only formed in the core and not in the cladding. This scheme provides the much needed degree of freedom to shift the Bragg condition to longer and more useful wavelengths, predominantly dependent on the angle between the interfering beams. A major step toward easier inscription of fiber gratings was made possible by the application of the phase mask as a tool for producing the interference pattern. The advantages of using a phase mask include the easier alignment and the low demand for the coherence of the optical source. The phase mask method then becomes the dominant method for fabricating FBGs. In order to write nonuniform gratings with advanced characteristics, one can use the scheme suggested by Stubbe et al [16][17].

1.2 The motivations of research

In order to demonstrate a direct method to measure the structure parameters of a fiber Bragg grating, we use the side diffraction interference method to measure the ac index modulation profile and the variation of the grating period. This direct axial scan technique can be use to real time monitor and control the grating growth during the writing process and determine the precise nature and location of defects along the fiber Bragg grating. In order to confirm the accuracies of the measured structure parameters, we use the transfer matrix method to simulate the reflection and transmission spectrum and compare them with those measured by the optical spectrum analyzer. Further more, we also use an indirect method called the discrete layer peeling to reconstruct the structure parameters from the reflection intensity and phase spectra of the fiber Bragg grating. The direct measured structure parameters are in consistent with the indirect reconstructed structure parameters. There is negligible danger of fiber damage when using the side diffraction interference method because no physical contact is made with the bare fiber.

1.3 The structure of this thesis

This thesis is consisted of four chapters. Chapter 1 is an introduction of the fiber Bragg gratings and their characterization techniques. Chapter 2 describes the theory and analysis of the experiment, i.e. couple mode equation, transfer matrix method, discrete layer peeling method, side diffraction interference, and phase measurement. Chapter 3 presents the experimental setup and results. Analyses of the results are also included. In chapter 4 we make a brief conclusion and discuss results that we have obtained.

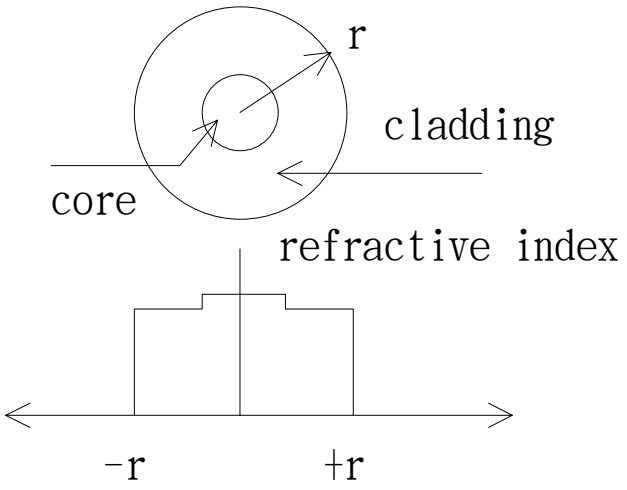

Fig.1.1 The refractive index profile of an optical fiber

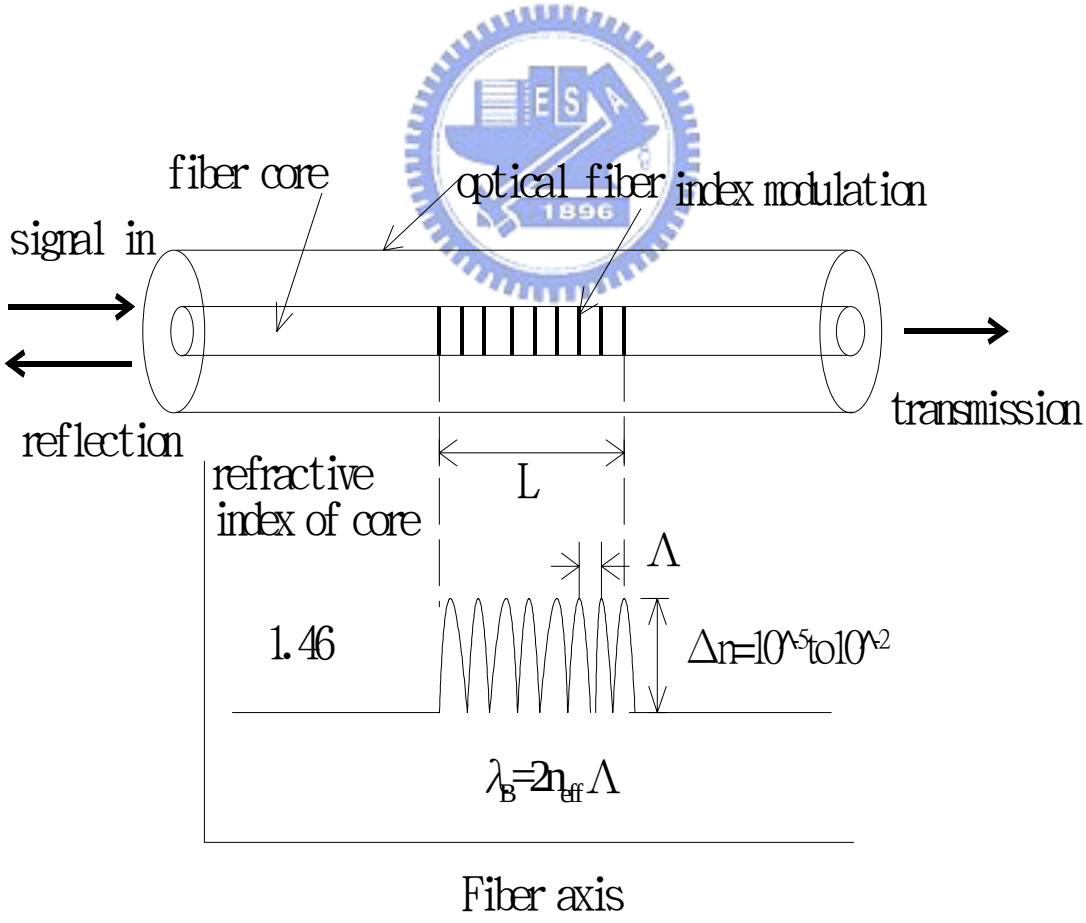

Fig.1.2 The refractive index modulation of fiber Bragg grating

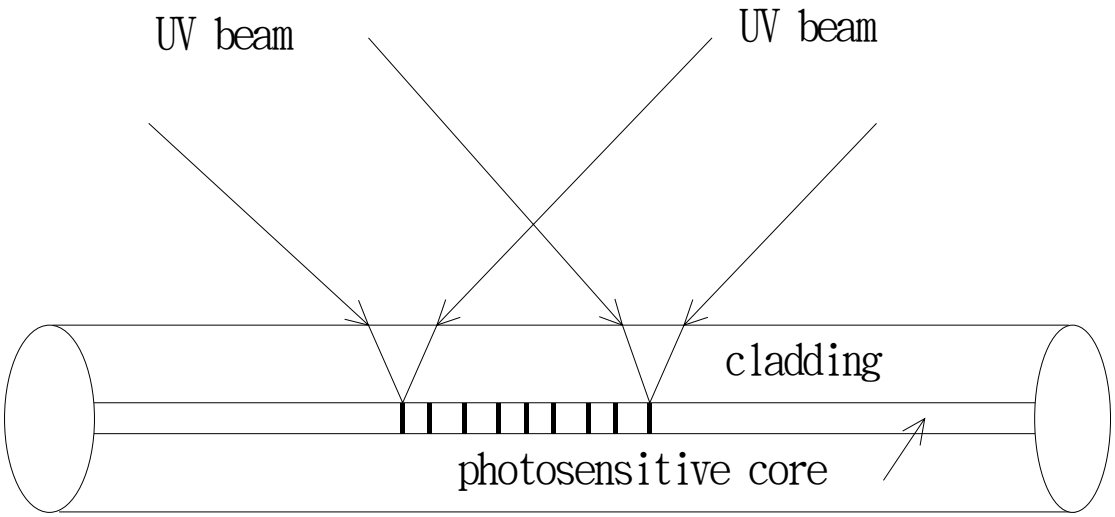

Fig.1.3 Writing the grating by exposing the fiber to UV interference from the side

Chapter 2 Analysis and experimental setup

2.1 Couple mode theory [22]

The relation between the spectral dependence of a fiber Bragg grating and the corresponding grating structure is usually described by the coupled mode theory. Coupled mode theory is described in a number of texts and the detailed analyses can be found in [10, 18, 19, 20, 21]. The axial refractive index of the fiber Bragg grating is represented by

$$n - \bar{n} = \Delta n_{ac}(z)\cos(\frac{2\pi}{\Lambda}z + \vartheta(z)) + \Delta n_{dc}(z) \tag{2.1}$$

as shown in Fig2.1. The coupled mode equation can be written as

$$\frac{du}{dz} = +i\delta u + q(z)v, \frac{dv}{dz} = -i\delta v + q^*(z)u \tag{2.2}$$

where u and v represent the forward and backward propagating modes respectively, $\delta = \beta - \pi/\Lambda$ is the wavenumber detuning, Λ is the grating period, and

$$|q(z)| = \eta\pi\Delta n_{ac}(z)/\lambda, \arg q(z) = \vartheta(z) - 2\eta k\int_0^z \Delta n_{dc}(z')dz' + \frac{\pi}{2} \tag{2.3}$$

Here $\Delta n_{ac}(z)$ and $\Delta n_{dc}(z)$ are the "ac" and "dc" index change respectively. The modulus of q is proportional to the index modulation amplitude or the peak to peak modulation of the index variation. The phase of q corresponds to the excess optical

phase or phase envelope of the grating. We can get q(z) from the structure parameter of the fiber Bragg grating and then use q(z) to simulate the reflection and transmission spectra by (2.2).

2.2 Transfer matrix method [22]

We divide the grating into a sufficient number of N sections so that each section can be approximately treated as a uniform grating. Let the section length be $\Delta = L/N$. By applying the appropriate boundary conditions and solving the coupled mode equations similar to the procedure above. We find the following transfer matrix relation between the fields at z and at z+ Δ

$$\begin{bmatrix} u(z+\Delta) \\ v(z+\Delta) \end{bmatrix} = \begin{bmatrix} \cosh(\gamma\Delta) + i\frac{\delta}{\gamma}\sinh(\gamma\Delta) & \frac{q}{\gamma}\sinh(\gamma\Delta) \\ \frac{q^*}{\gamma}\sinh(\gamma\Delta) & \cosh(\gamma\Delta) - i\frac{\delta}{\gamma}\sinh(\gamma\Delta) \end{bmatrix} \begin{bmatrix} u(z) \\ v(z) \end{bmatrix}. \quad (2.4)$$

Hence, we can connect the fields at the two ends of the grating through

$$\begin{bmatrix} u(L) \\ v(L) \end{bmatrix} = T \begin{bmatrix} u(0) \\ v(0) \end{bmatrix}, T = T_N * T_{N-1} * .....T_1, \quad (2.5)$$

where T is the overall transfer matrix. The matrix T_j is the transfer matrix written in (2.4) with $q = q_j = q(j\Delta)$, the coupling coefficient of the jth section. As a result, T is a 2*2 matrix with elements

$$T = \begin{bmatrix} T_{11} & T_{12} \\ T_{21} & T_{22} \end{bmatrix}. \quad (2.6)$$

Once T is found, the reflection coefficient and the transmission coefficient are calculated by the relations

$$r(\delta) = -T_{21}/T_{22}, t(\delta) = 1/T_{22}, \tag{2.7}$$

which are obtained by the substitution of the appropriate boundary conditions into (2.5)

2.3 Discrete layer peeling method [22]

One can replace the matrix T by the product of two transfer matrixes $T_\Delta T_\rho$. One of them (T_ρ) describes a discrete reflector, and the other (T_Δ) describes the pure propagation of the fields,

$$T_\rho = (1-|\rho|^2)^{-1/2}\begin{bmatrix} 1 & -\rho^* \\ -\rho & 1 \end{bmatrix}, T_\Delta = \begin{bmatrix} \exp(i\delta\Delta) & 0 \\ 0 & \exp(-i\delta\Delta) \end{bmatrix}, \tag{2.8}$$

here the discrete, complex reflection coefficient is given by

$$\rho = -\tanh(|q|\Delta)\frac{q^*}{|q|}. \tag{2.9}$$

The discrete model of the entire grating is thus a series of N discrete, complex reflectors with a distance Δ between all reflectors. We will define the forward and backward propagating fields before the jth section as $u_j(\delta)$ and $v_j(\delta)$ (see Fig(2.2)). For numerical implementation, the spectral dependence must also be discretized, and hence the calculation of ρ_1 by the inverse fourier transform of $r_1(\delta)$ can be achieved by the discrete fourier transform

$$\rho_1 = \frac{1}{M}\sum_{m=1}^{M} r_1(m), \tag{2.10}$$

where $r_1(m)$ denotes a discrete version of the spectrum $r_1(\delta)$ in the range $|\delta| \le \pi/2\Delta$, and $M \ge N$ is the number of wavelengths in the spectrum. Note that

Eq(2.10) is valid for all layers by substituting 1→j in the subscripts, because the reference plane is transferred to the actual layer through

$$r_2(\delta) = \exp(-i2\delta\Delta)\frac{r_1(\delta) - \rho_1}{1 - \rho^*_1 r_1(\delta)} \tag{2.11}$$

The discrete layer peeling algorithm can be summarized in the following simple steps:

i) Start with the target reflection intensity spectrum(R(δ)) and reflection phase spectrum(φ(λ))

ii) Compute ρ_1 from Eq(2.10)

iii) Propagate the fields using Eq(2.11)

iv) Repeat step ii) until the entire grating structure is detemined.

v) Compute the coupling coefficient q_j by

$$\left|q_j\right| = \frac{-1}{2\Delta}\ln\left(\frac{1-\left|\rho_j\right|}{1+\left|\rho_j\right|}\right), \arg(q_j) = -\arg(\rho_j) \tag{2.12}$$

2.4 Experimental setup and analysis for side diffraction interference [23][24][25]

2.4.1 Experimental setup

Figure 2.3 and 2.4 shows the two experimental setups demonstrated in the thesis for the characterization of the fiber Bragg gratings. The difference between the two setups is that the setup1 has a higher spatial resolution than the setup2, but in contrast we can detect the variation of the grating period only by using setup2. Although there is little difference between these two setups, the principles of them are the same. The light source is a cw laser (here a He-Ne laser operating at a wavelength of λ = 632.8nm). A polarization beam splitter is used to split the laser beam into a probe beam and a reference beam. Two half-wave-plates produce nearly perfect s-polarized beams and allow the ratio of the intensities of the two beams to be adjusted when the first half wave plate is rotated. In this way, substantially more intensity can be provided to the probe beam, which will generate the first order diffracted beam with quite low efficiency, depending on the grating strength. In addition, an attenuator can be used to achieve an even larger ratio of I_p/I_r to yield a high fringe visibility. In the setup1 the probe beam is focused by a spherical lens of 20cm focal length onto the side of the fiber Bragg grating, so the FWHM width of the probe beam measured along the fiber axis is 80 μm. In the setup2 the probe beam is focused by a cylindrical lens of 30cm focal length onto the side of the fiber Bragg grating, so the FWHM width of the probe beam measured along the fiber axis is 1.5mm which is identical to the beam width of the He-Ne laser source. Because the probe beam width of setup1 measured along the fiber axis is much smaller than that of setup2. the spatial resolution of the setup1 is larger than the spatial resolution of the setup2. The angle of the incidence satisfies the Bragg condition. We find the condition for Bragg reflection of the probe beam by

matching the grating vector K with the difference of the axial components of the incident (i) and reflected (r) wave vectors, $k_{i,z} - k_{r,z} = K = \frac{2\pi}{\Lambda}$. As the transmitted and the reflected beams leave the fiber at the opposite sides of the fiber at equal angles $\pm\theta_r$, we have

$$k_{i,z} - k_{r,z} = K = \frac{2\pi}{\Lambda} \Rightarrow (\frac{2\pi}{\lambda}\sin\vartheta_i) - (-\frac{2\pi}{\lambda}\sin\theta_r) = \frac{2\pi}{\Lambda}, \vartheta_i = \vartheta_r \Rightarrow \sin\theta_r = \frac{\lambda}{2\Lambda} = N_B \lambda/\lambda_B$$

(2.13)

Here N_B is the effective index of the fiber at the retroreflected Bragg wavelength $\lambda_B = 2\Lambda N_B$. The calculated angle of incidence is $\theta_i \fallingdotseq 36.2568$(deg). The fiber Bragg grating is held horizontally in a pair of clamps separated by 30 cm, which can be translated along the fiber axis by a translation stage and PZT. The probe beam produces first order diffracted beam after it passes through the grating. In the setup1 the diffracted beam is refocused by another spherical lens of 20cm focal length, but not in the setup2. The purpose of using another spherical lens in the setup1 is to produce a plane wave in the horizontal plane and than the period of interference pattern will be a constant. A monochrome CCD camera of 7.15-um pixel width is used to record the fringe pattern. A computer data acquisition system controlled by the Labview program is used to save the images of the interference pattern and to perform the required analysis. By scanning the fiber Bragg grating we can measure the ac index profile and the variation of the grating period. As described in 2.3.2, the ac index modulation of the FBG in the probed area, Δn_{ac}, can be inferred from the total radiation power detected by the CCD or from the amplitude of the interference pattern.

The change in the grating period, $\Delta\Lambda$, can be measured from the change in the period of the interference fringes.

2.4.2 Analysis [23][24][25]

We assume that the fiber Bragg grating to be measured is approximately uniform across the fiber core of diameter 2a and has a sinusoidal index variation of amplitude Δn_{ac} along the fiber axial direction z. The fringes of the grating are represented by a spatial modulation of the core refractive n(z) as

$$n(z) = n_{core} + \Delta n_{dc}(z) + \Delta n_{ac}(z)\cos(\frac{2\pi}{\Lambda}z), \tag{2.14}$$

where n_{core} is the refractive index of core, $\Delta n_{dc}(z)$ is the dc index profile, $\Delta n_{ac}(z)$ is the ac index profile, Λ is the grating period. The intensity of the first order diffracted beam (with intensity I_p) is denoted I_d, and the intensity of the reference beam is denoted I_r. The diffraction efficiency η of the grating for the first order diffracted beam is

$$\eta = \frac{|E_d|^2}{|E_p|^2} = \frac{I_d}{I_p} = c^2 \Delta n_{ac}{}^2, \tag{2.15}$$

when Bragg condition is satisfied, where c is a constant of proportionality defined for convenience. The power of the diffracted beam is denoted P_d.

$$P_d \propto I_d \propto \Delta n_{ac}{}^2. \tag{2.16}$$

The interference of the diffracted beam and the reference beam is given by

$$I_{inter} = I_d + I_r + 2\sqrt{I_d I_r}\cos(2\pi fx) = c^2 \Delta n_{ac}{}^2 I_p + I_r + 2\sqrt{c^2 \Delta n_{ac}{}^2 I_p I_r}\cos(2\pi fx) \quad , \tag{2.17}$$

where f is the spatial frequency of the interference fringe pattern and $f = 1/\lambda_{inter}$. Here λ_{inter} is the period of the interference fringe pattern. We perform the Fourier transform of the interference fringe patterns, then use a filter to select the interference term $2\sqrt{c^2 \Delta n_{ac}{}^2 I_p I_r}\cos(2\pi fx)$. The amplitude of this term is proportional to Δn_{ac} and the angle α between the two interference beams is given by

$$\alpha = 2\sin^{-1}\left(\frac{\frac{2\pi}{\lambda_{inter}}/2}{\frac{2\pi}{\lambda}}\right) = 2\sin^{-1}\left(\lambda f/2\right). \tag{2.18}$$

With the phase matching condition along the axis of the FBG, the variation of the grating period can be represented by

$$\frac{2\pi}{\lambda}\sin\theta + \frac{2\pi}{\lambda}\sin(\theta+\alpha) = \frac{2\pi}{\Lambda} \Rightarrow \frac{2\pi}{\lambda}\sin\theta + \frac{2\pi}{\Lambda}\sin\theta + \frac{2\pi}{\lambda}\cos\theta\sin\alpha = \frac{2\pi}{\Lambda} \Rightarrow$$
$$\frac{2\pi}{\Lambda} = \frac{4\pi}{\lambda}\sin\theta + \frac{2\pi}{\lambda}\cos\theta\sin\alpha = \frac{4\pi}{\lambda}\sin\theta\left(1+\frac{\alpha}{2\tan\theta}\right) \Rightarrow \Lambda = \frac{\lambda}{2\sin\theta}\left(1-\frac{\alpha}{2\tan\theta}\right) \tag{2.19}$$

The requirement that $\alpha << 1$, which also corresponds to $\lambda f / 2 << 1$, simply implies that the two beams are nearly parallel and hence give rise to interference fringes that are spaced by the distance much larger than the wavelength of the He-Ne laser. Using Eq.(2.28), we can then write the local grating period with respect to the central period Λ_0 as

$$\Lambda \approx \Lambda_0 - (\Lambda_0 \frac{\lambda}{2\tan\theta}) f \ . \tag{2.20}$$

Therefore the relative variation in the grating period, $\Delta\Lambda$, is given by the expression

$$\Delta\Lambda = \frac{\Lambda\lambda}{2\tan\theta} f \ . \tag{2.21}$$

Equation (2.16) and (2.17) form the basis for evaluating the ac index modulation Δn_{ac}, and equation (2.21) forms the basis for evaluating grating period variation $\Delta\Lambda$.

The whole analysis process is shown below

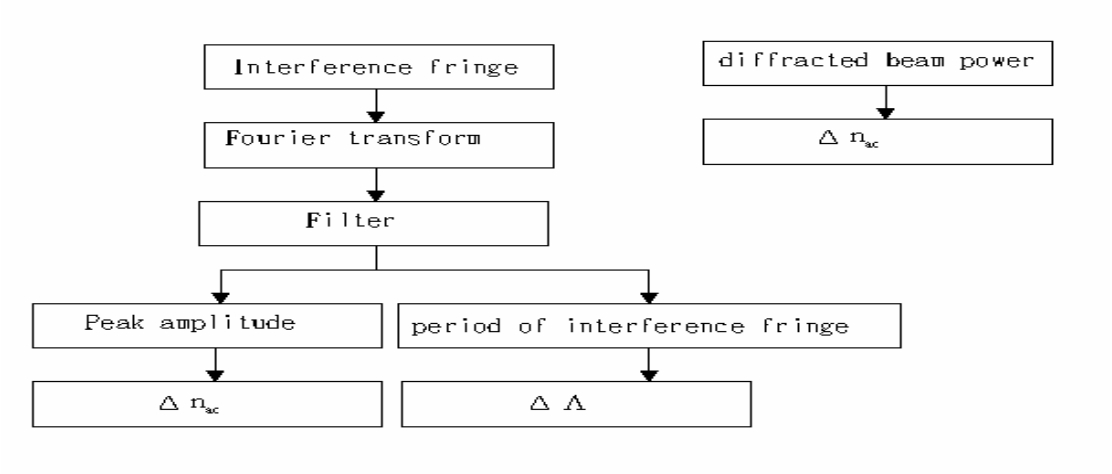

2.5 Experimental setup and analysis for phase measurement[26]

For performing analyses for the whole optical properties of fiber Bragg gratings, we not only have to obtain the reflection intensity spectrum, but also the phase spectrum of the reflection light. To get the reflection intensity spectrum we just have to use a broad band source and an optical spectrum analyzer. On the other hand, the phase information can not be performed simply. Figure 2.5 shows the experiment setup demonstrated in this thesis for the phase spectrum measurement of the fiber Bragg grating. The setup is a typical Michelson interferometer. The broad-band light from the Er-fiber ASE (Amplified Spontaneous Emission) source is split after passing through a 50/50 coupler. The signal beam is reflected by a fiber Bragg grating and carries the phase information of the grating. The reference is reflected by a reflection mirror after emerging from a collimator. The two beams form the interference pattern after passing through 50/50 coupler. We use an optical spectrum analyzer to observe the interference fringe. The optical path reflected from the grating is denoted path1. The optical field of the path1 can be represented as

$$\widetilde{E}_1(\lambda) = E_1(\lambda)\exp(i\frac{2\pi}{\lambda}n_{eff}L_1 + i\Phi(\lambda)). \tag{2.22}$$

Let $I_{grating} = \left\langle \widetilde{E}_1^{\,2} \right\rangle$, Φ is the phase delay induced by grating, which is also the phase of the $r = |r|\exp(i\Phi)$ in Equation (2.7). L_1 is the length of the path1. The optical field of the path2 is represented by

$$\widetilde{E}_2(\lambda) = E_2(\lambda)\exp(i\frac{2\pi}{\lambda}n_{eff}L_2). \tag{2.23}$$

Let $I_{reference} = \left\langle \tilde{E}_2^{\,2} \right\rangle$, The reflection mirror is almost dispersionless near the wavelength of 1550nm. L_2 is the length of the path2. The interference of the two beams can be represented as

$$\begin{aligned} I_{inter}(\lambda) &= \left\langle \tilde{E}_1^{\,2}(\lambda) \right\rangle + \left\langle \tilde{E}_2^{\,2}(\lambda) \right\rangle + \left\langle \tilde{E}_1(\lambda) * \tilde{E}_2^{\,*}(\lambda) \right\rangle + \left\langle \tilde{E}_2(\lambda) * \tilde{E}_1^{\,*}(\lambda) \right\rangle \\ &= I_{grating} + I_{reflect} + 2\sqrt{I_{reflect} * I_{grating}} \cos(\frac{2\pi}{\lambda} n_{eff} l + \varphi) \end{aligned}, \qquad (2.24)$$

where $l = L_1 - L_2$, which is the difference of the lengths of the two paths. A typical interference fringe pattern is shown in Fig2.6. We then make the fourier transform of the I_{inter} and plot the absolute value of it, as shown in Fig2.7. The phase information is encoded in the ac signals. In order to get φ, we use a filter window to filter out the positive frequency ac signal. The bandwidth of the window (filter) will affect the measured group time delay. Generally speaking, the group time delay will oscillate when the bandwidth is large, whereas the result will be smooth when the bandwidth is small. The reason is that the use of a large bandwidth filter will include in more high frequency noises. We shift the ac signal to dc and perform the inverse Fourier transform to get $\sqrt{I_{reflect} I_{grating}} \exp(i\varphi)$. By extracting the phase term we obtain the phase spectrum of the fiber Bragg grating. The length of the path1 should be longer than the length of the path2. If the length of the path2 is longer than the length of the path1, Equation (3.3) would become

$$I_{inter}(\lambda) = I_{grating} + I_{reflect} + 2\sqrt{I_{reflect} * I_{grating}} \cos(\frac{2\pi}{\lambda} n_{eff} * (-l) + (-\varphi)). \qquad (3.4)$$

Then the phase we obtain is $-\varphi$. If the length of the path1 is equal to the length of the path2, after we make the fourier transform of I_{inter}, $I_{grating}$, $I_{reflect}$ and $2\sqrt{I_{reflect} * I_{grating}} * \cos(\frac{2\pi}{\lambda} * 0 + \varphi)$ would become mixed and we will not be able to separate them apart. After getting the phase spectrum of the grating, we can evaluate the group delay by the expression below.

$$t = -\frac{\lambda^2}{2\pi c}\frac{d(\varphi(\lambda))}{d\lambda} \quad . \tag{3.5}$$

The whole process of analysis is shown below.

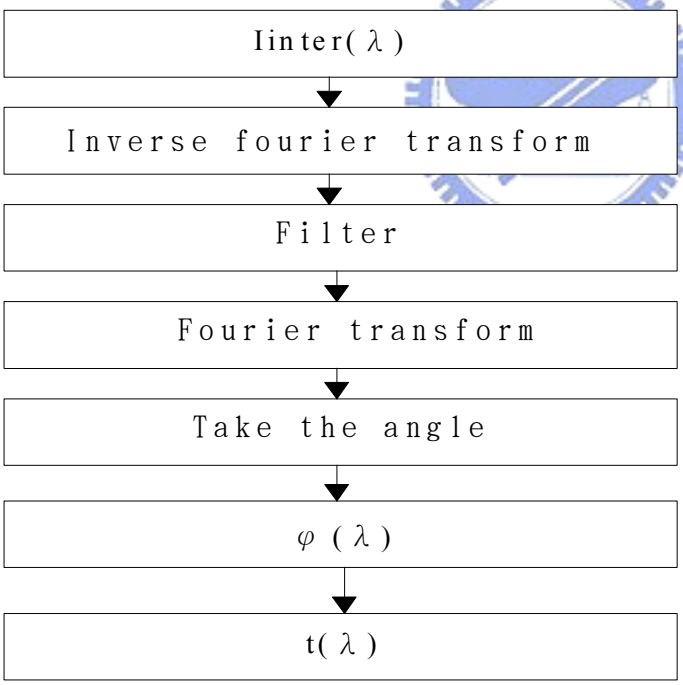

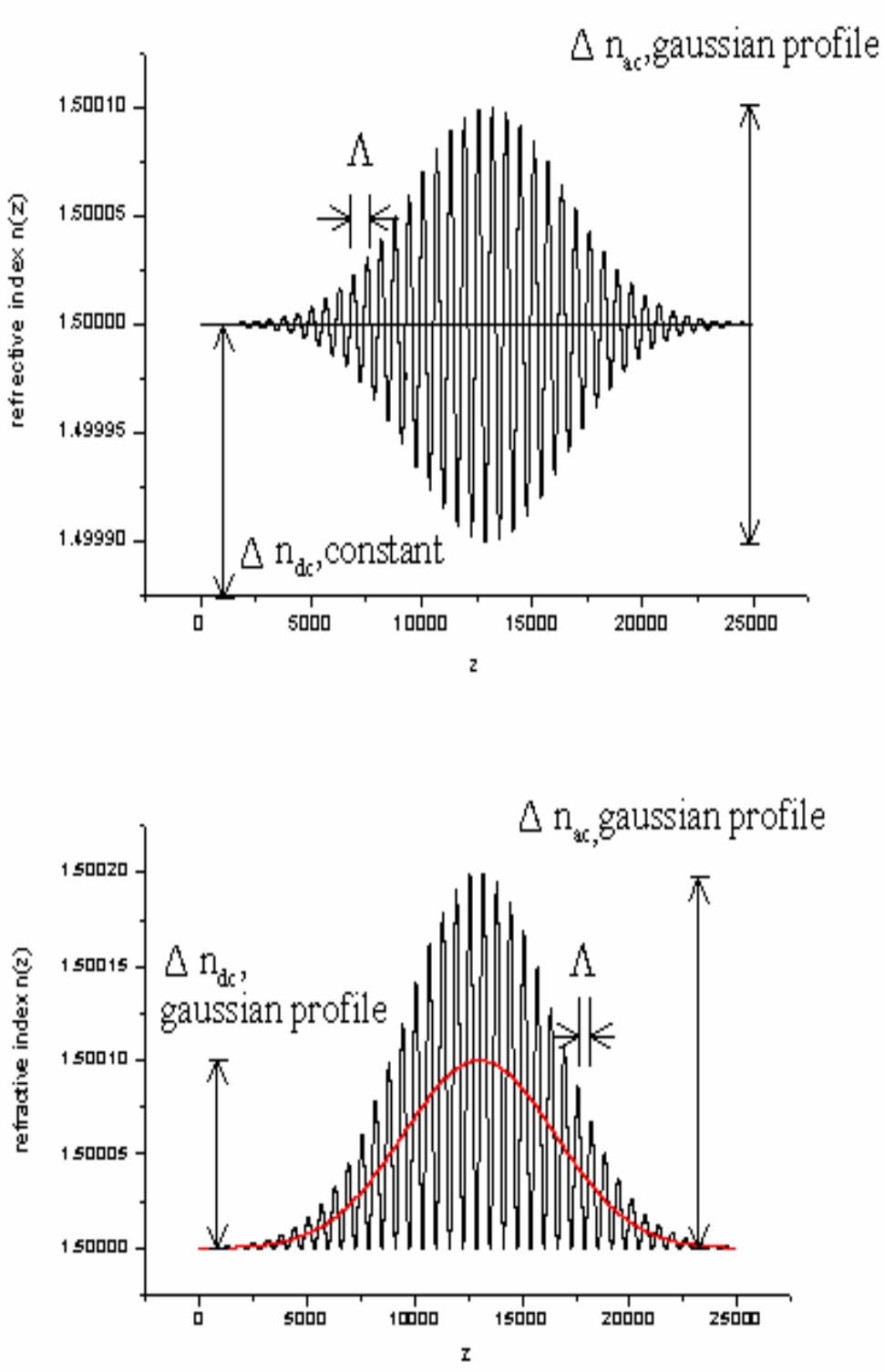

Fig.2.1 Ac and dc index modulation of two fiber Bragg gratings

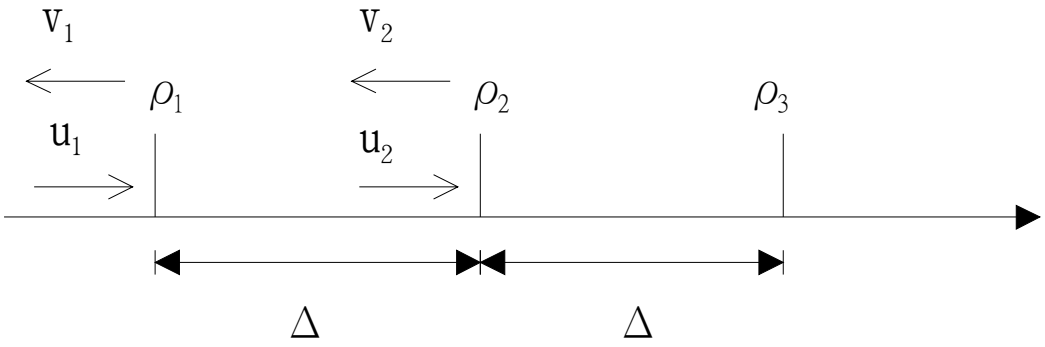

Fig.2.2 The discrete model of fiber Bragg grating

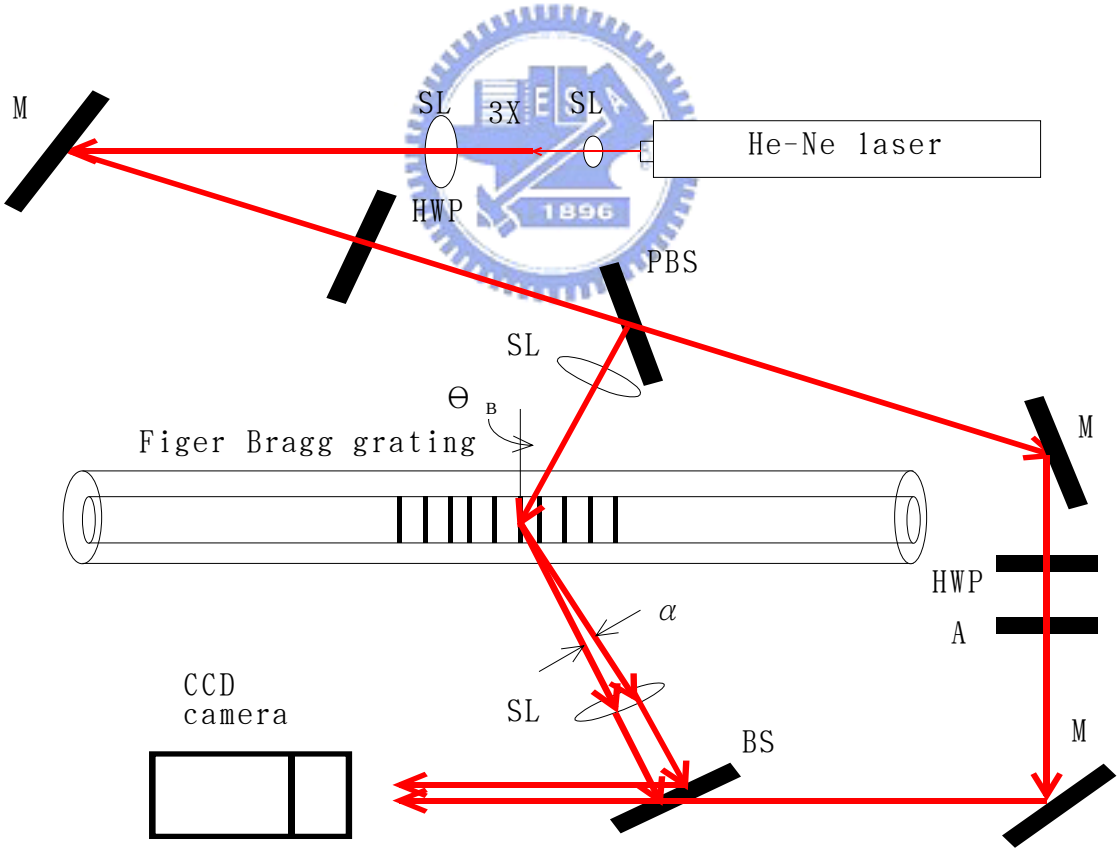

Fig.2.3 Setup1 for side diffraction interference

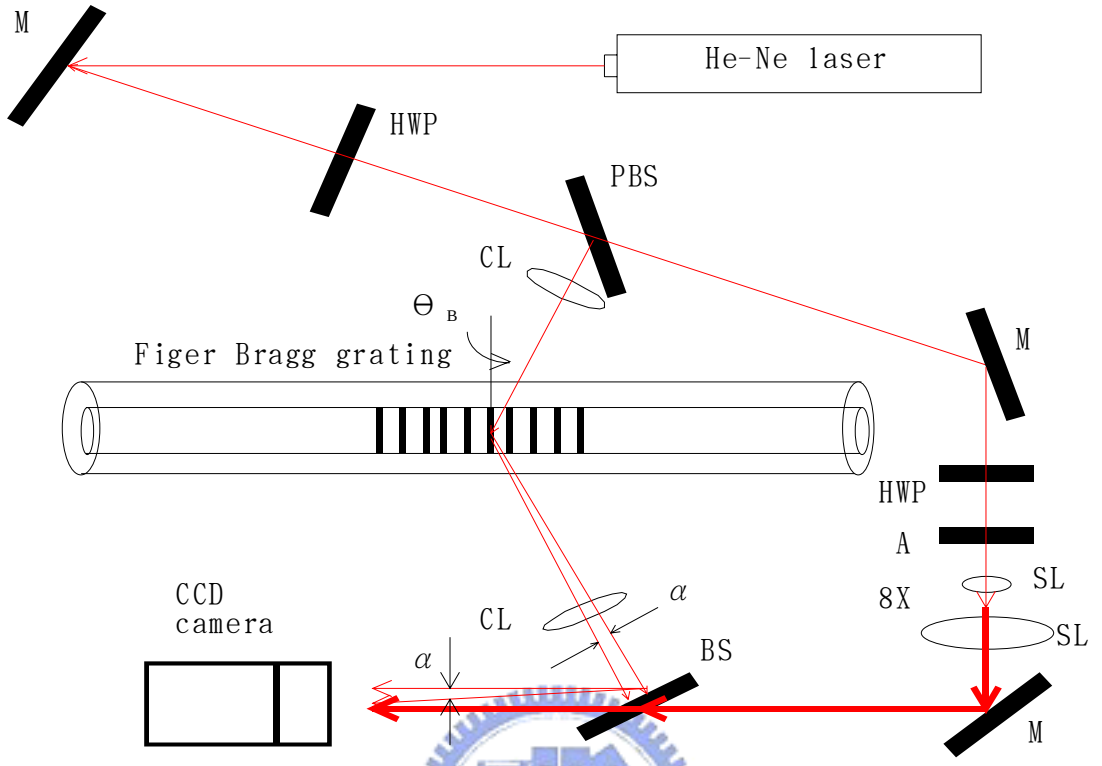

Fig.2.4 Setup2 for side diffraction interference

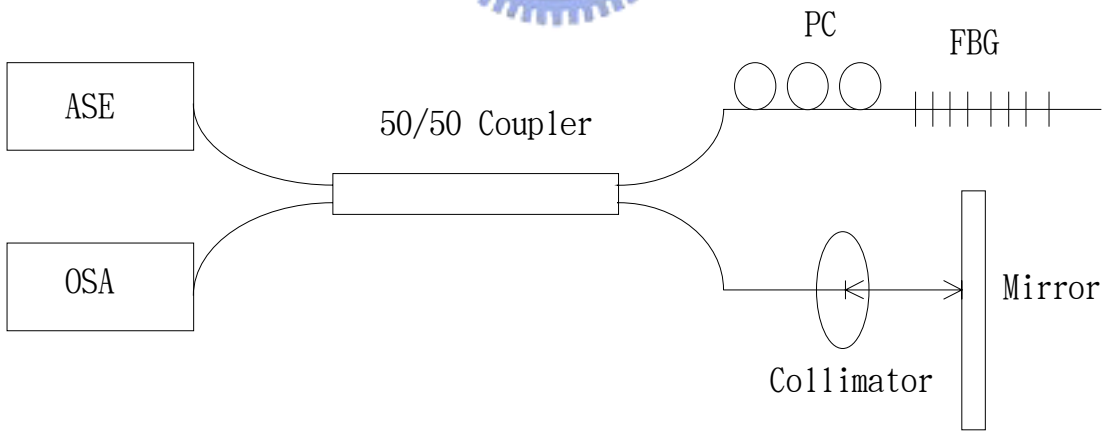

Fig.2.5 Setup for the phase measurement of the fiber Bragg grating

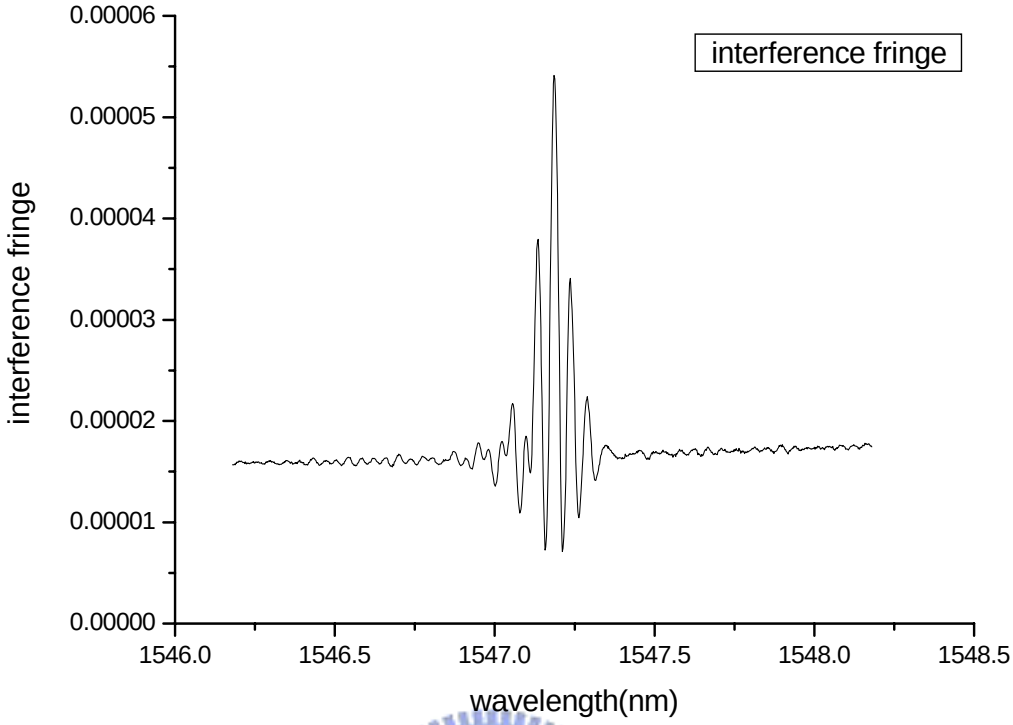

Fig.2.6 Interference fringe from optical spectrum analyzer

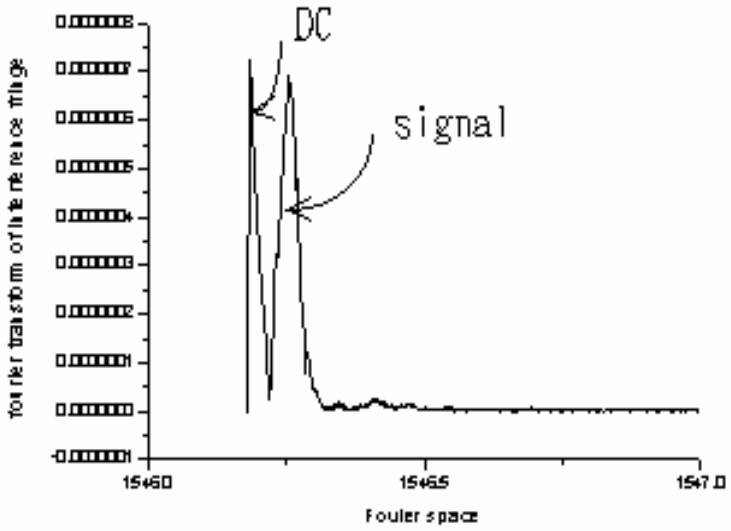

Fig.2.7 The Fourier transform of the interference fringe

Chapter 3 Experimental results

3.1 Experimental results of side diffraction interference

3.1.1 3dB Gaussian apodized grating

A 3dB Gaussian apodized grating made by a uniform phase mask is studied first. The power of the first order diffracted beam along the fiber axis is measured by the side diffraction method and the measurement results are shown in Figure 3.1. Because the intensity distribution of the UV laser beam is a Gaussian profile. We can see that the measured side diffraction ac index profile is also a Gaussian profile. The e^{-1} width of the UV beam is about 6.4~7.1cm and the e^{-1} width of the measured profile is about 7cm. The total width of the UV beam is about 20cm and the total width of the measured profile is about 10.5cm. By Fourier transforming the interference pattern and get the peak amplitude of the ac term we obtain the side interference ac index, as shown in Figure 3.2. Fig 3.2 also shows the repetibility of the measurement. The e^{-1} width of the side interference ac index profile is about 8cm and the total width of that is about 13cm. We can see that the side interference method can detect smaller index amplitudes the than side diffraction method, as shown in Figure 3.3.

The period of the interference pattern(CCD pixel) measured along the fiber axis is also measured. By $\Delta\Lambda = \frac{\Lambda\lambda}{2\tan\theta} f$, $f = \frac{1}{\lambda_{inter}}$ we can obtain the side interference grating period and the results are shown in Figure 3.4. The grating period distribution along the grating is almost a constant, in consistence with the use of the uniform phase mask. The resolution of the grating period measurement is about 0.01nm.

3.1.2 5dB linear chirp Gaussian apodized grating

A 5dB linear chirp Gaussian apodized grating made by a uniform phase mask is then characterized. The power of the first order diffracted beam along the fiber axis is measured, and the results of side diffraction method are shown in Figure 3.5. Because the intensity distribution of the UV laser beam is a Gaussian profile. We can see that the measured side diffraction ac index profile is also a Gaussian profile. The e^{-1} width of the UV beam is about 6.4~7.1cm and the e^{-1} width of the measured profile is about 6.5cm. The total width of the UV beam is about 20cm and the total width of the measured profile is about 10.5cm. By performing Fourier transform of the interference pattern and get the peak amplitude of the ac term we obtain the side interference ac index, as shown in Figure 3.6. Fig 3.6 also shows the repetibility of the measurement. The e^{-1} width of the side interference ac index profile is about 7.5cm and the total width of that is about 12cm. Again we can see that the side interference method can detect smaller index variation than the side diffraction method as shown in Figure 3.7.

The period of the interference pattern(CCD pixel) measured along the fiber axis is measured, and the results are shown in Figure 3.8. The grating period distribution along the grating is linearly increased, in consistence with the use of the linear phase mask. The chirp rate of the measured grating period is 0.7049/1.22 = 0.5778(nm/cm) and the linear chirp rate of the phase mask is 0.5(nm/cm).

3.2 Simulation results of transfer matrix method

3.2.1 3dB Gaussian apodized grating

The ac index profile of the 3dB Gaussian apodized grating made by the uniform phase mask is used to simulate the corresponding reflection and transmission spectra by transfer matrix method. First we use the side diffraction ac index profile as shown in Figure 3.1. Because the power of +1 and -1 order beam is 70% of the total power, we represent the dc refractive index profile as $n_{dc}(z) = n_{core} + \frac{4}{3}\Delta n_{ac}(z)$. When $\Delta n_{ac,max}$ = 0.00005925, the simulated transmission spectrum and the transmission spectrum measured by the optical spectrum analyzer are shown in Figure 3.9. The simulated reflection spectrum and the reflection spectrum measured by the optical spectrum analyzer are shown in Figure 3.10. The reflection and transmission spectra simulated by the transfer matrix method and the structure parameters obtained are in good agreement with those measured by optical spectrum analyzer. Then by fitting the curve in Figure 3.1, we obtain the fitting side diffraction ac index as shown in Figure 3.11. With the same procedure above, when $\Delta n_{ac,max}$ = 0.000062, the simulated transmission spectrum from the fitting result and the simulated transmission spectrum in Figure 3.9 are compared as shown in Figure 3.12. The simulated reflection spectrum from the fitting result and the simulated reflection spectrum in Figure 3.10 are compared as shown in Figure 3.13. We can observe that the difference of the two spectra in Fig 3.12 and 3.13 is only the height of the side lobes in the longer wavelength region. The similarity between them shows that the optical performance of many fiber Bragg grating devices are only affected by errors that occur over a relatively large (millimeter) length scale.

Next we use the side interference ac index profile as shown in Figure 3.2. When $\Delta n_{ac,max}$ = 0.000054, the simulated transmission spectrum and the transmission spectrum measured by the optical spectrum analyzer are shown in Figure 3.14. The simulated reflection spectrum and the reflection spectrum measured by the optical spectrum analyzer are shown in Figure 3.15. The reflection and transmission spectra simulated by the transfer matrix method and the structure parameters obtained are in good agreement with those measured by optical spectrum analyzer. Then by fitting the curve in Figure 3.2 we obtain the fitting side interference ac index as shown in Figure 3.16. With the same simulation model above, when $\Delta n_{ac,max}$ = 0.00005, the simulated transmission spectrum from the fitting result and the simulated transmission spectrum in Figure 3.14 are compared as shown in Figure 3.17. The simulated reflection spectrum from the fitting result and the simulated reflection spectrum in Figure 3.15 are compared as shown in Figure 3.18. We can observe that the difference of the two spectra in Fig 3.17 and 3.18 is only the height of the side lobes in the longer wavelength region. The similarity between them shows that the optical performance of many fiber Bragg grating devices are only affected by errors that occur over a relatively large (millimeter) length scale..

3.2.2 5dB linear chirp Gaussian apodized grating

The ac index profile of the 5dB linear chirp Gaussian apodized grating made by the linear phase mask is also used to simulate the corresponding reflection and transmission spectra by transfer matrix method. First we use the side diffraction ac index profile as shown in Figure 3.5 and the side interference grating period as shown in Figure 3.8. Again we represent the dc refractive index profile as $n_{dc}(z) = n_{core} + \frac{4}{3}\Delta n_{ac}(z)$. When $\Delta n_{ac,max}$ = 0.000218, the simulated transmission spectrum and the transmission spectrum measured by optical spectrum analyzer are shown in Figure 3.19. The simulated reflection spectrum and the reflection spectrum measured by optical spectrum analyzer are shown in Figure 3.20. The reflection and transmission spectra simulated by the transfer matrix method and the structure parameters obtained are again in good agreement with those measured by optical spectrum analyzer. Then by fitting the curves in Figure 3.5 and 3.8 we obtain the fitting the side diffraction ac index and the fitting side interference grating period as shown in Figure 3.21. With the same procedure above, when $\Delta n_{ac,max}$ = 0.00022, the simulated transmission spectrum from the fitting result and the simulated transmission spectrum in Figure 3.19 are compared as shown in Figure 3.22. The simulated reflection spectrum from the fitting result and the simulated reflection spectrum in Figure 3.20 are compared as shown in Figure 3.23. Like 3.2.1 we can observe that the difference of the two spectra in Fig 3.22 and 3.23 is only the height of side lobes in the longer wavelength region. The similarity between them again shows that the optical performance of many fiber Bragg grating devices are only affected by errors that occur over a relatively large (millimeter) length scale.

Next we use the side interference ac index profile as shown in Figure 3.6 and side interference grating period as shown in Figure 3.8. When $\Delta n_{ac,max}$ = 0.0002325, the simulated transmission spectrum and the transmission spectrum measured by the optical spectrum analyzer are shown in Figure 3.24. The simulated reflection spectrum and the reflection spectrum measured by the optical spectrum analyzer are shown in Figure 3.25. The reflection and transmission spectra simulated by the transfer matrix method and the structure parameters obtained are in good agreement with those measured by optical spectrum analyzer. Then by fitting the curve in Figure 3.6 and 3.8 we obtain the fitting side interference ac index and the fitting side interference grating period as shown in Figure 3.26. With the same simulation model and procedure above, when $\Delta n_{ac,max}$ = 0.0002225, the simulated transmission spectrum from the fitting curve and the simulated transmission spectrum in Figure 3.24 are compared as shown in Figure 3.27. The simulated reflection spectrum from the fitting curve and the simulated reflection spectrum in Figure 3.25 are compared as shown in Figure 3.28. We can observe that the difference of the two spectra in Fig 3.27 and 3.28 is only the height of the side lobes in the longer wavelength region. The similarity between them shows that the optical performance of many fiber Bragg grating devices are only affected by errors that occur over a relatively large (millimeter) length scale once again.

3.3 Experiment results of phase measurement

3.3.1 3dB Gaussian apodized grating

The phase spectrum of the 3dB Gaussian apodized grating by the uniform phase mask is shown in Fig 3.29. The group delay spectrum is shown in Fig 3.30.

3.3.2 5dB linear chirp Gaussian apodized grating

The phase spectrum of the 5dB linear chirp Gaussian apodized grating by the linear phase mask is then shown in Fig 3.31. The group delay spectrum is shown in Fig 3.32.

3.4 Reconstruction results by discrete layer peeling

3.4.1 3dB Gaussian apodized grating

The ac index profile of the 3dB Gaussian apodized grating by the uniform phase mask is reconstructed by the discrete layer peeling method and is shown in Fig 3.33. The target reflection spectrum and the reflection spectrum obtained by the discrete layer peeling method are shown in Fig 3.34. The target and the reconstructed phase spectra are shown in Fig 3.35.

3.4.2 5dB linear chirp Gaussian apodized grating

The ac index profile of the 5dB linear chirp Gaussian apodized grating by the linear phase mask is reconstructed by the discrete layer peeling method and the result is shown in Fig 3.36. The target reflection spectrum and the reflection spectrum obtained by the discrete layer peeling method are shown in Fig 3.37. The target and the reconstructed phase spectra are shown in Fig 3.38.

3.5 Comparison of the ac index profile from side diffraction interference and discrete layer peeling

3.5.1 3dB Gaussian apodized grating

The ac index profile of the 3dB Gaussian apodized grating by the side diffraction and the discrete layer peeling is shown in Fig 3.39. The ac index profile of the 3dB Gaussian apodized grating by the side interference and the discrete layer peeling is shown in Fig 3.40. We can observe that the values of Δn_{max} in Fig 3.39 and 3.40 are close. Both of them have a dip in the center of the profile. Unfortunately, because the phase measurement is not accurate enough for a uniform grating, the reconstructed ac index profile is longer than the ac index profile measured by the side diffraction interference method.

3.5.2 5dB linear chirp Gaussian apodized grating

The ac index profile of the 5dB linear chirp Gaussian apodized grating by the side diffraction and the discrete layer peeling is shown in Fig 3.41. The ac index profile of the 5dB linear chirp Gaussian apodized grating by the side interference and the discrete layer peeling is shown in Fig 3.42. We can observe that the values of Δn_{max} in Fig 3.41 and 3.42 are quite the same. The shapes of Fig 3.39 and 3.40 are also quite close. The total lengths of the profiles from the side diffraction interference method and the discrete layer peeling method are also about the same.

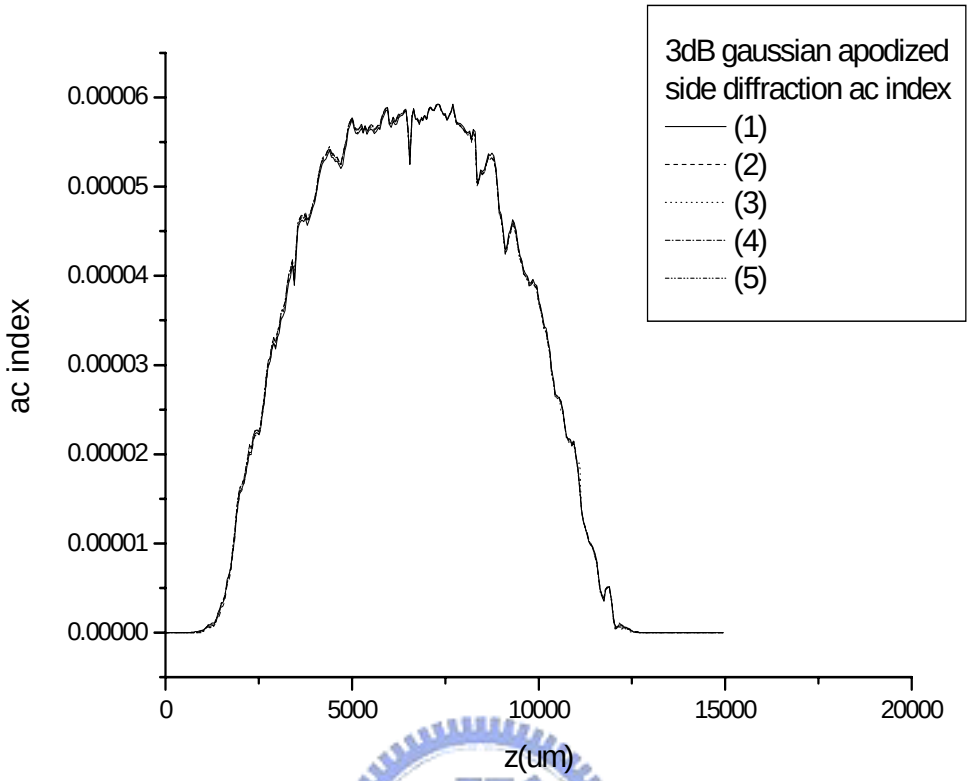

Fig.3.1 Side diffraction ac index of 3dB Gaussian apodized grating

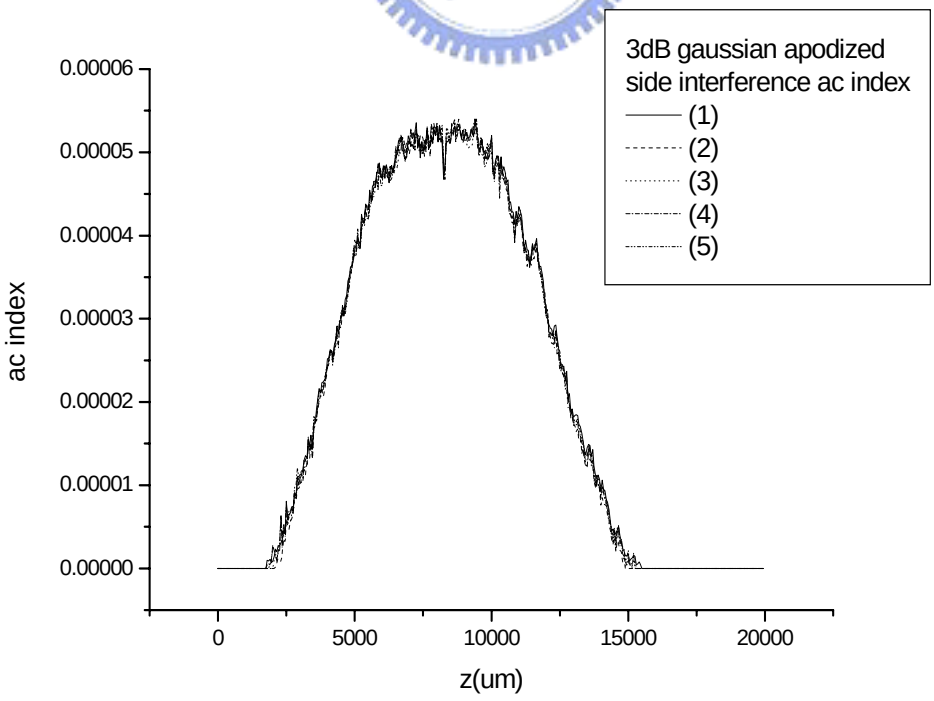

Fig.3.2 Side interference ac index of 3dB Gaussian apodized grating

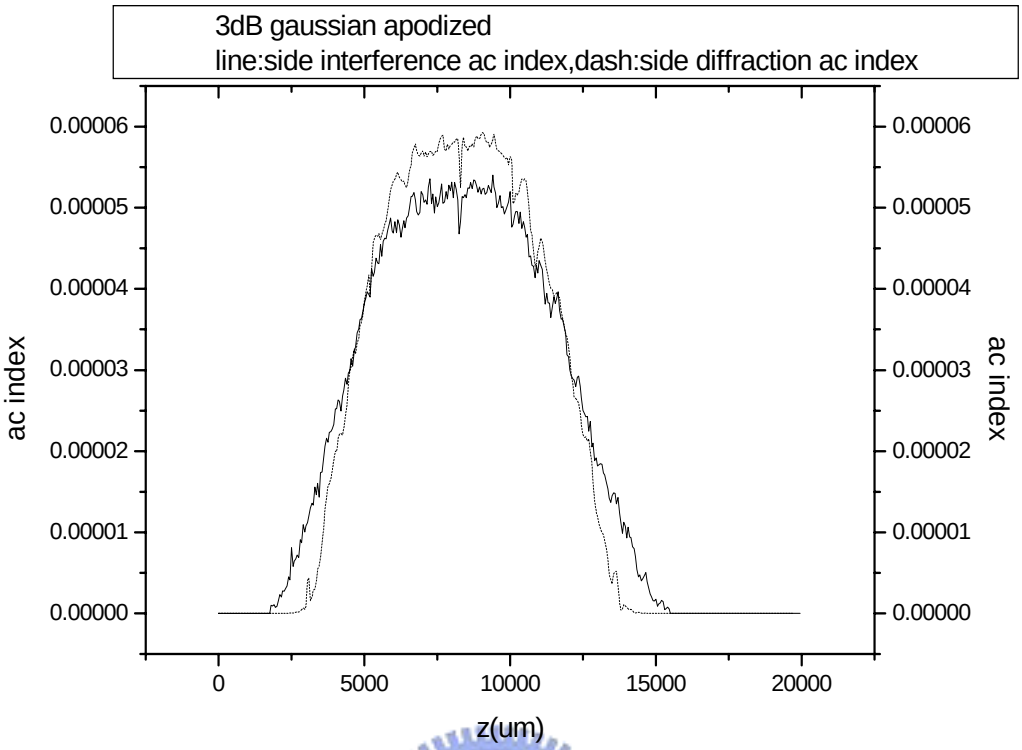

Fig.3.3 The comparison between side diffraction and side interference ac index

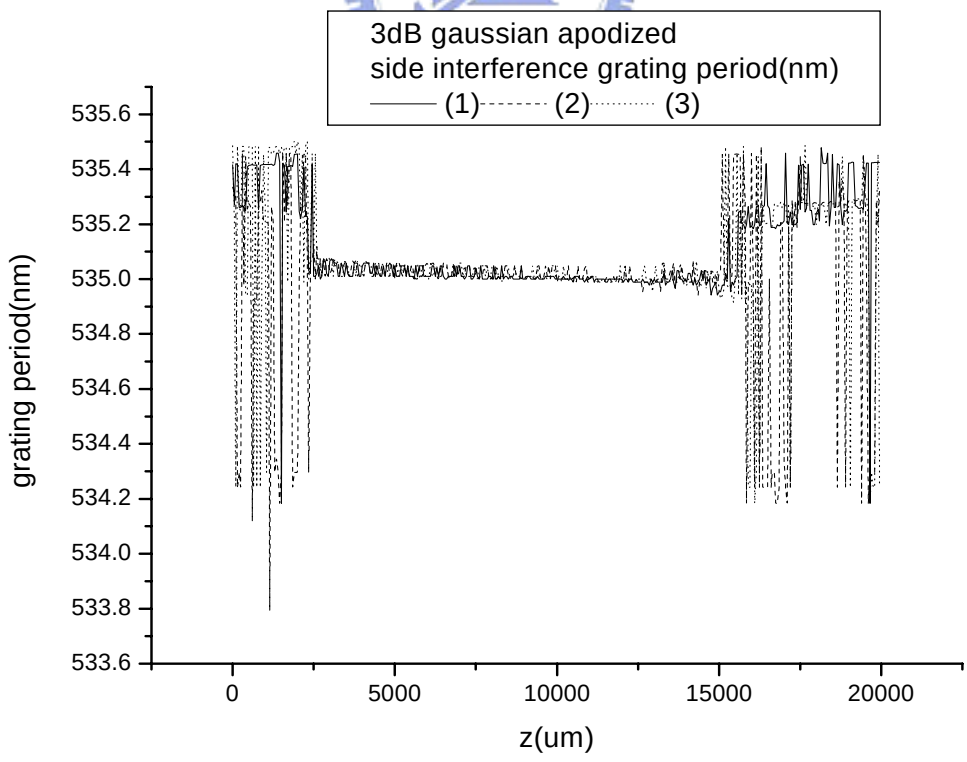

Fig.3.4 Grating period of 3dB Gaussian apodized grating

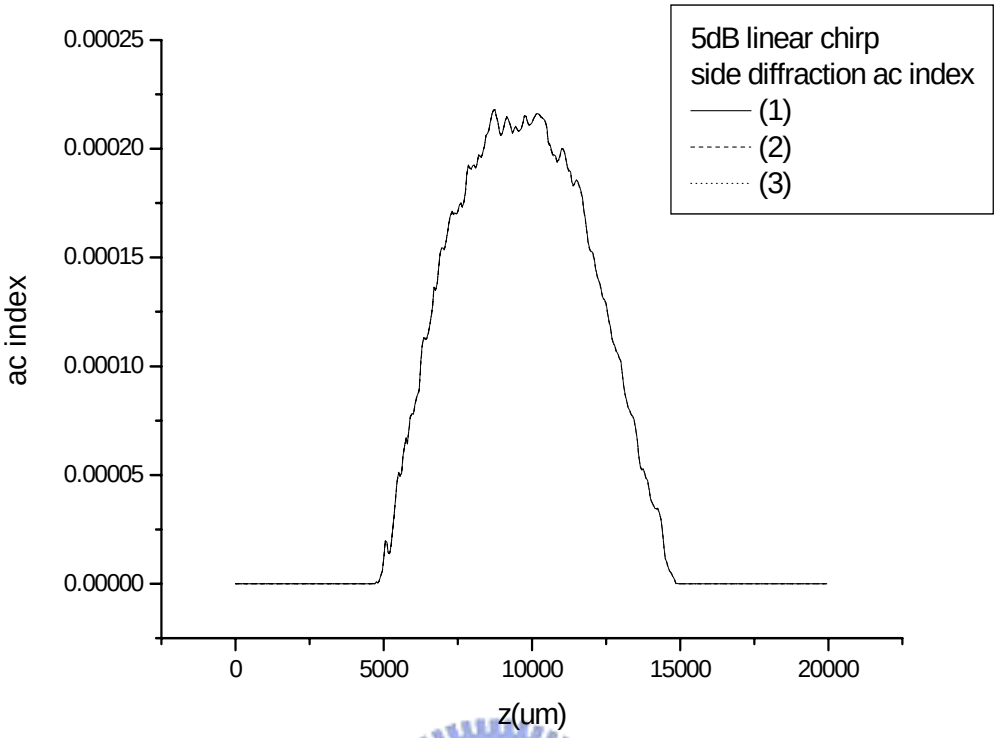

Fig.3.5 Side diffraction ac index of 5dB linear chirp grating

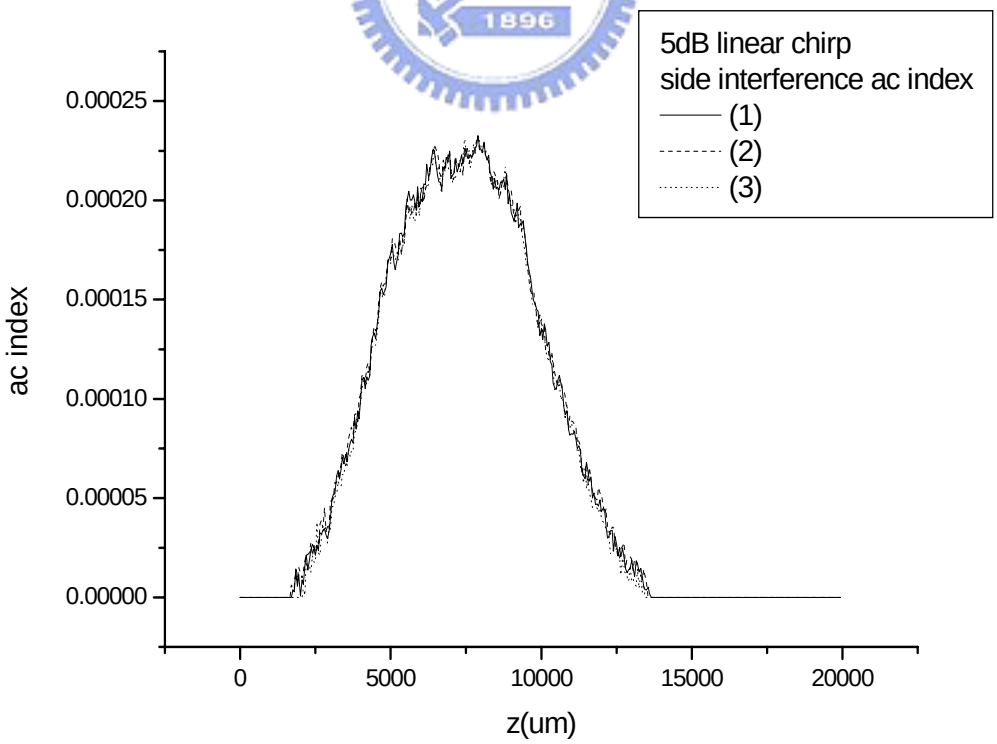

Fig.3.6 Side interference ac index of 5dB linear chirp grating

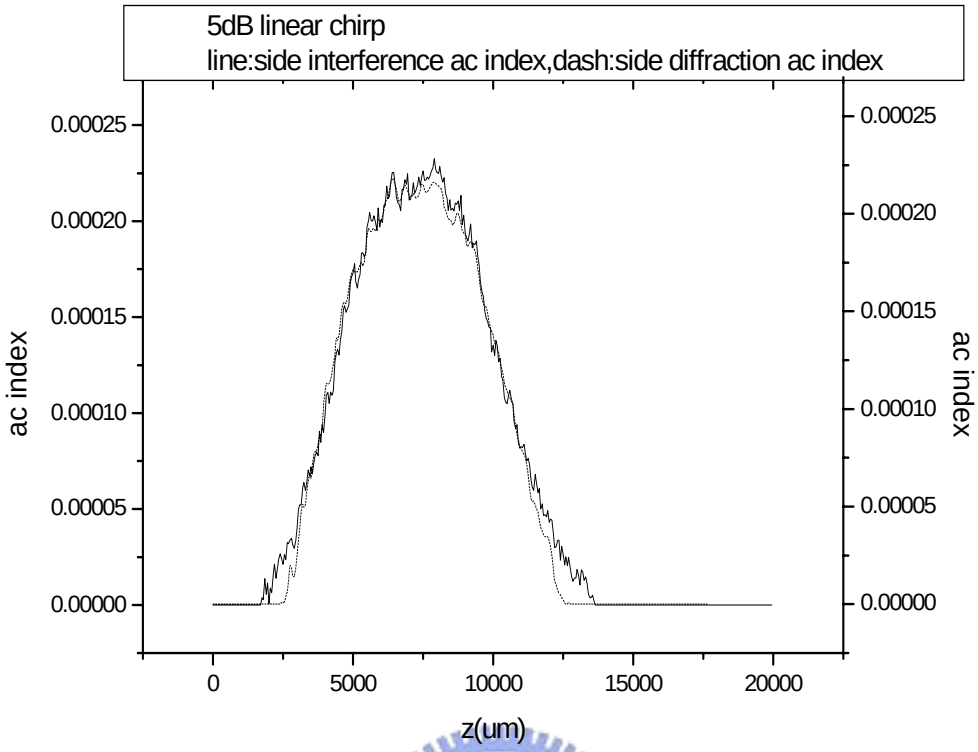

Fig.3.7 The comparison between side diffraction and side interference ac index

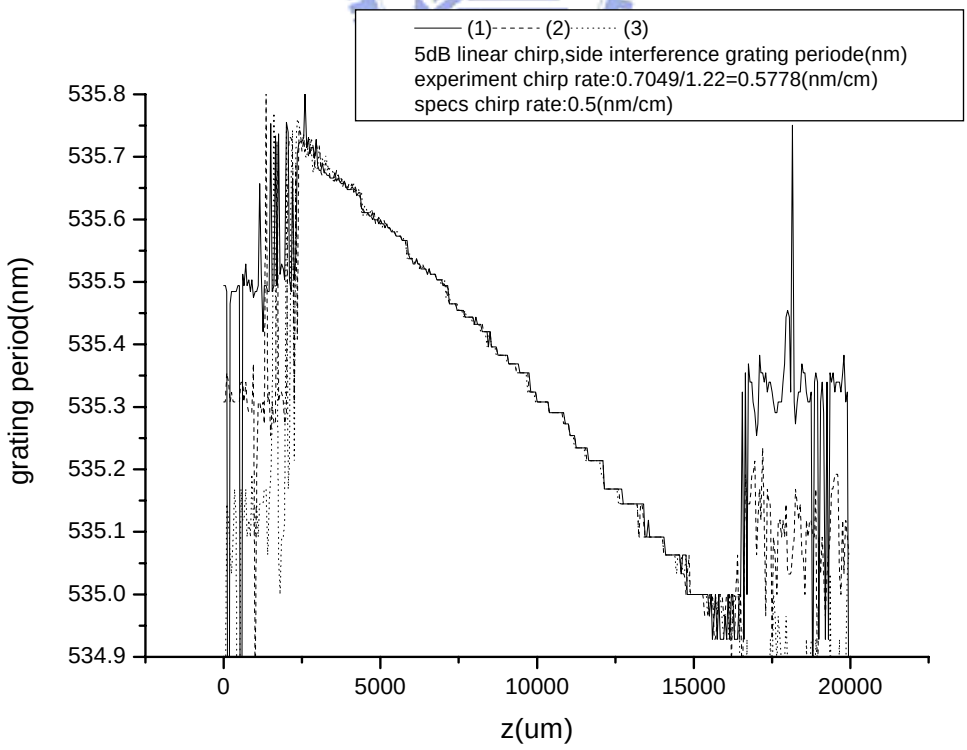

Fig.3.8 Grating period of 5dB linear chirp grating

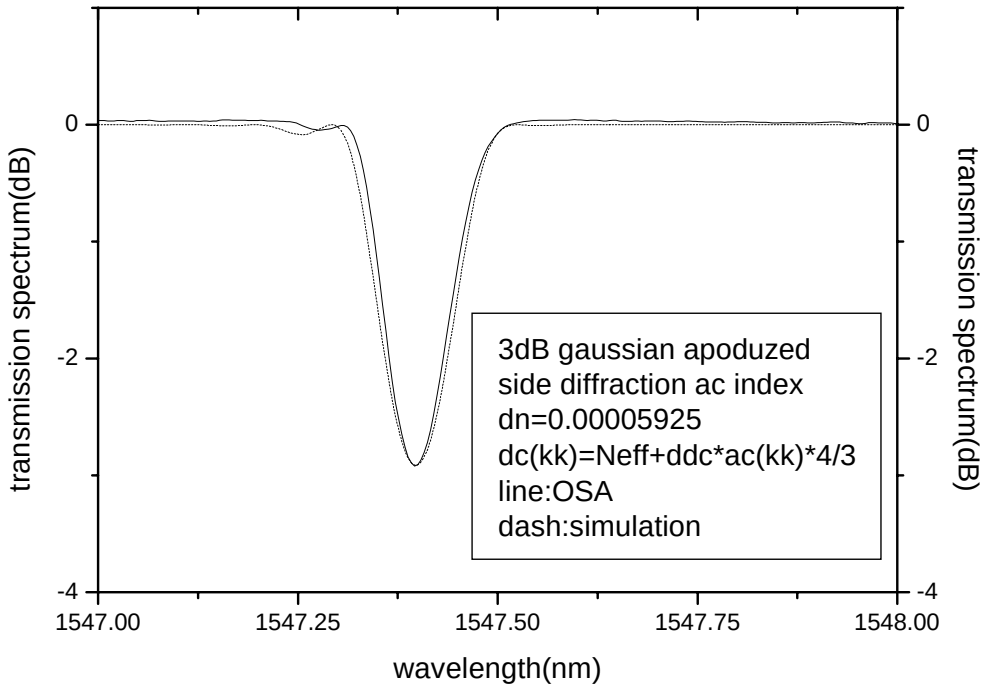

Fig.3.9 Transmission spectrum by simulation and by OSA

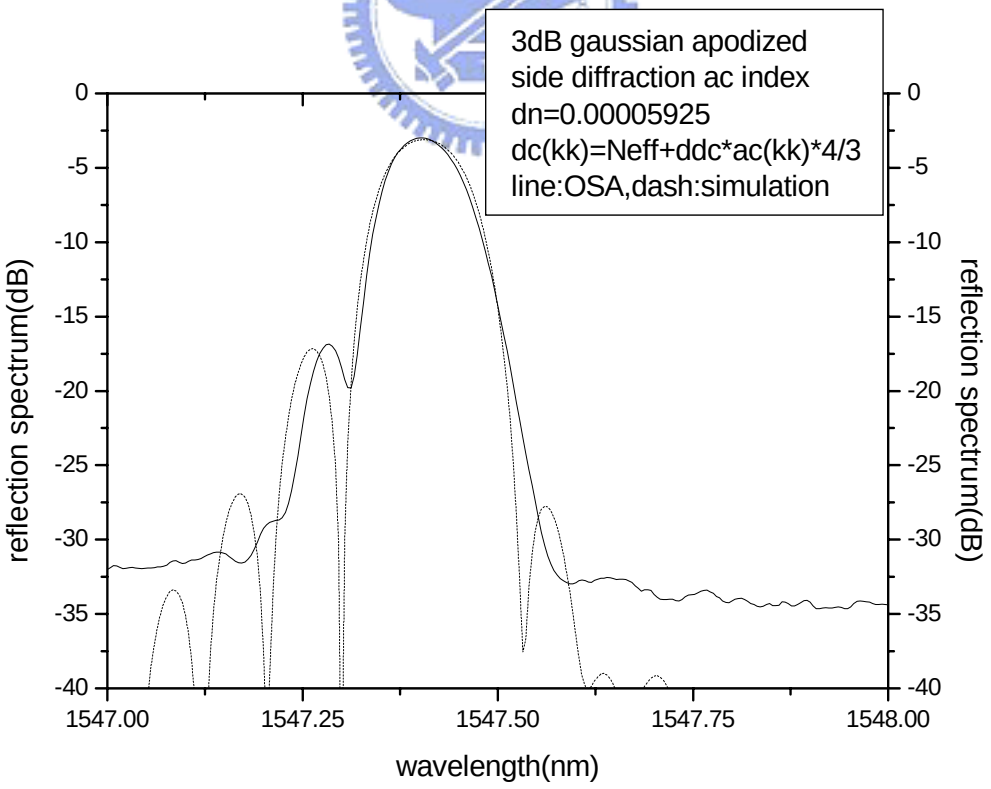

Fig.3.10 Reflection spectrum by simulation and OSA

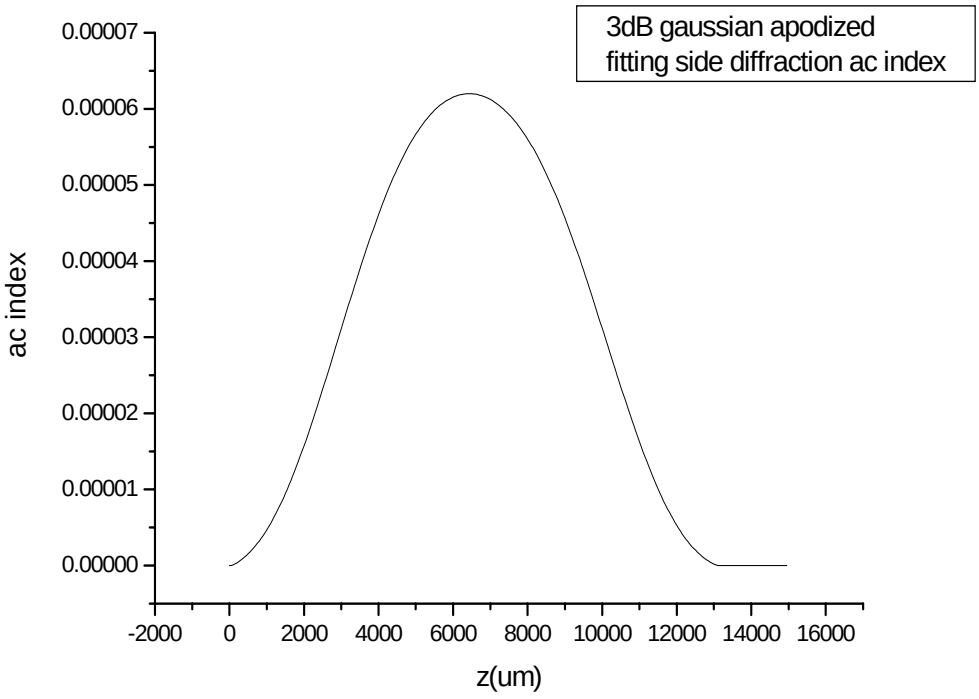

Fig.3.11 Fitting side diffraction ac index

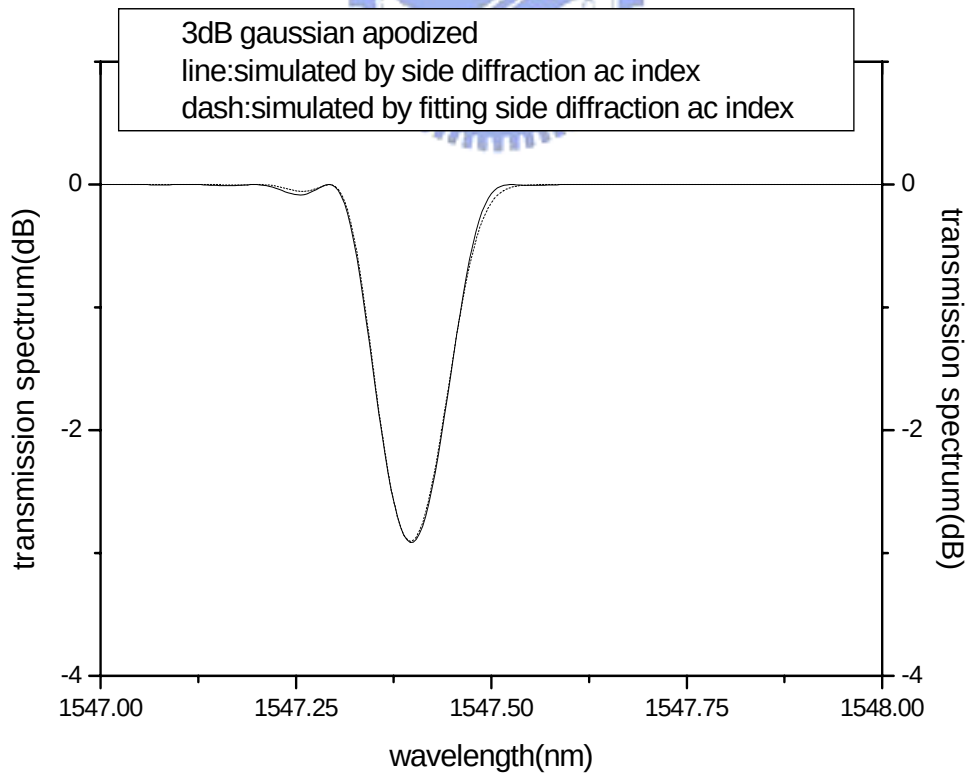

Fig.3.12 Simulated transmission spectra

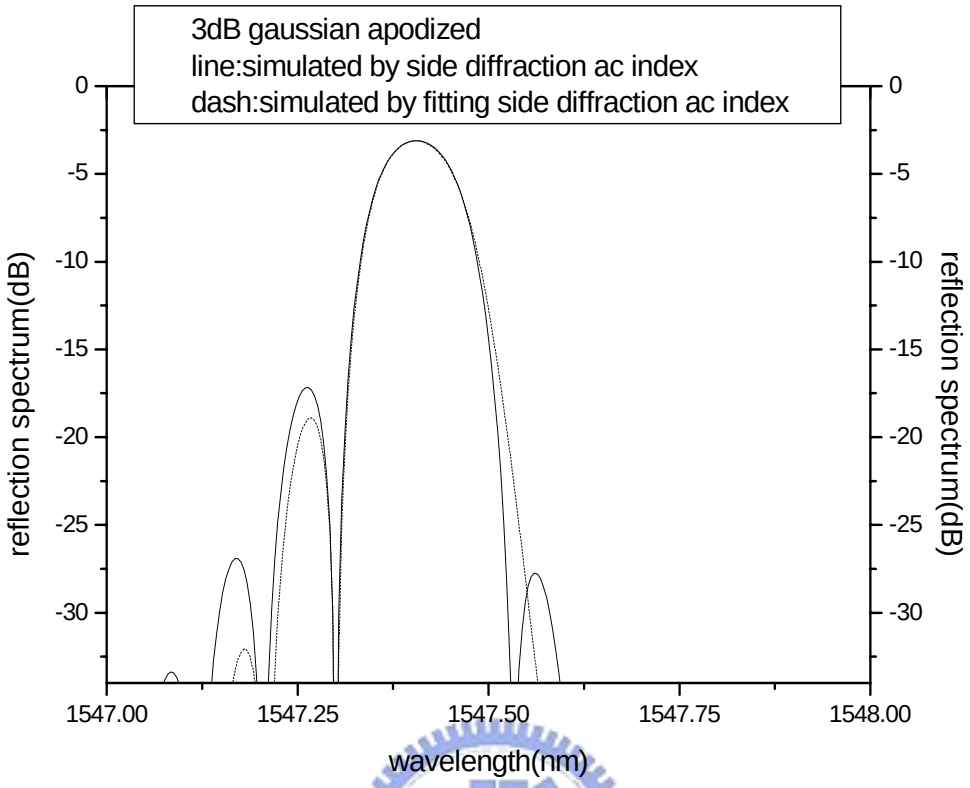

Fig.3.13 Simulated reflection spectra

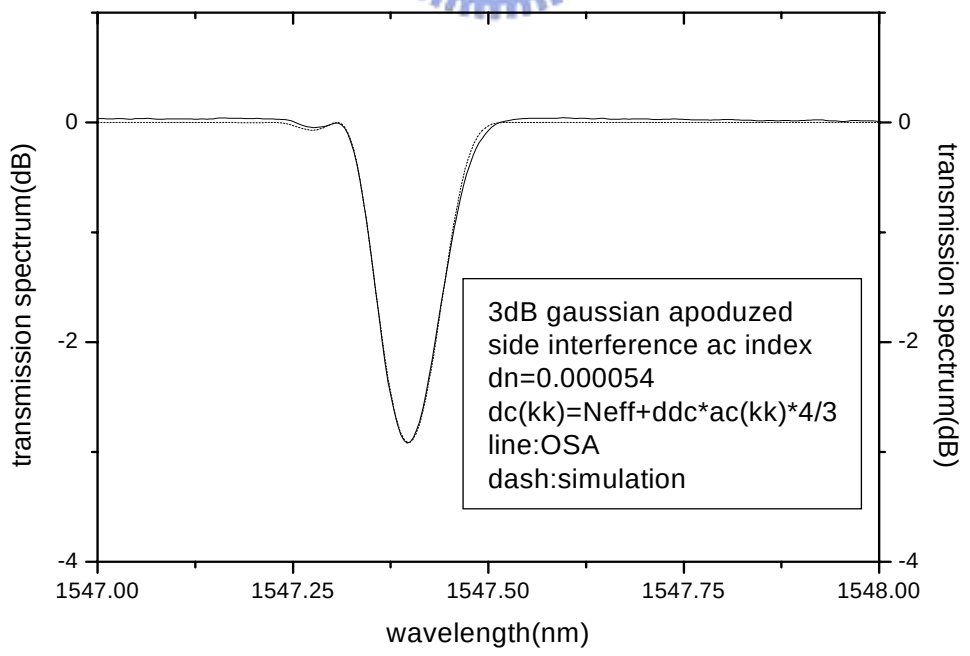

Fig.3.14 Transmission spectrum by simulation and by OSA

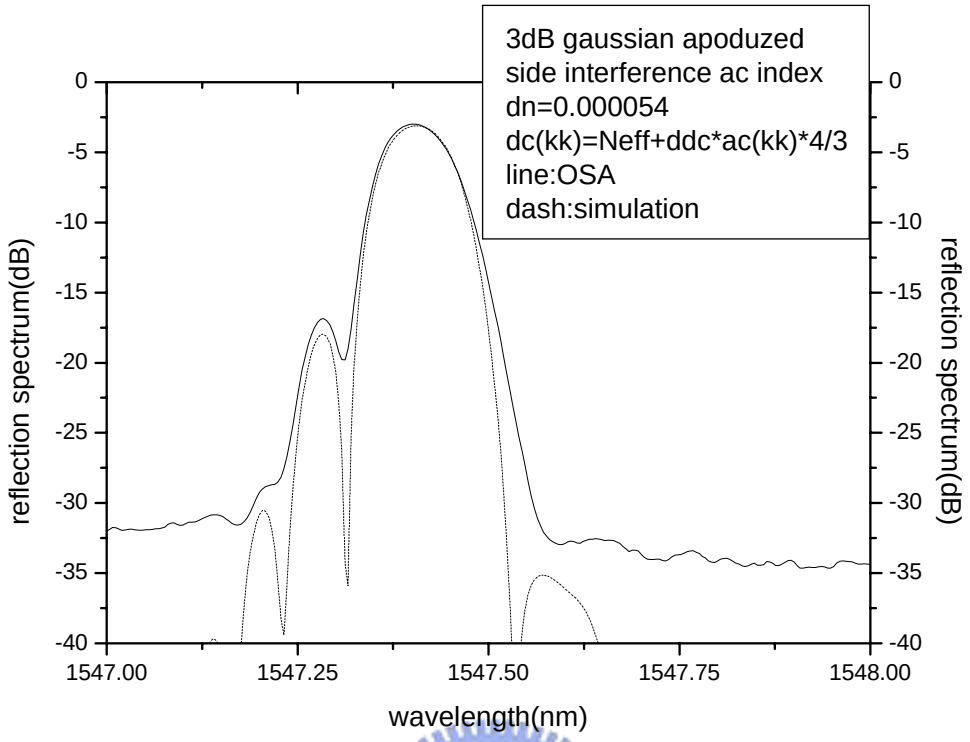

Fig.3.15 Reflection spectrum by simulation and OSA

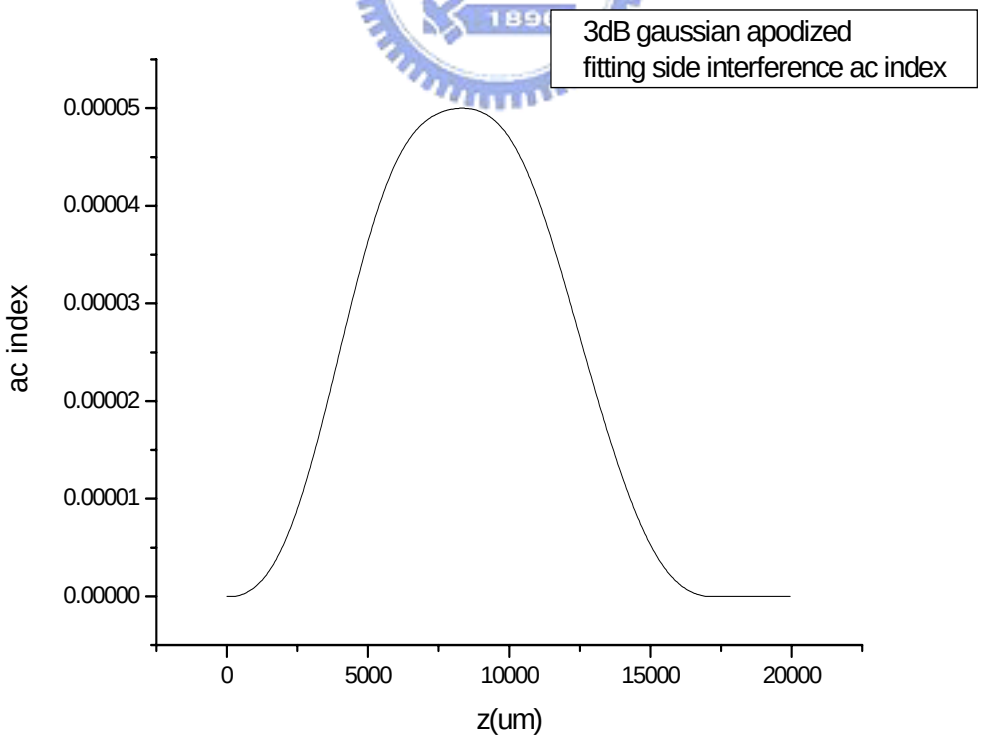

Fig.3.16 Fitting side interference ac index

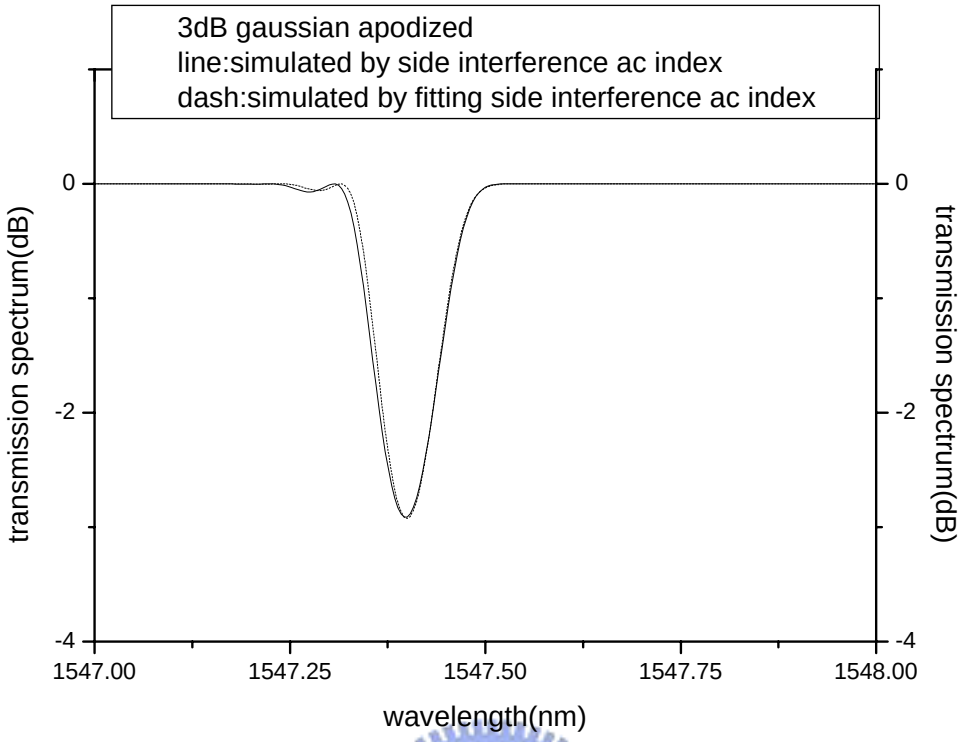

Fig.3.17 Simulated transmission spectra

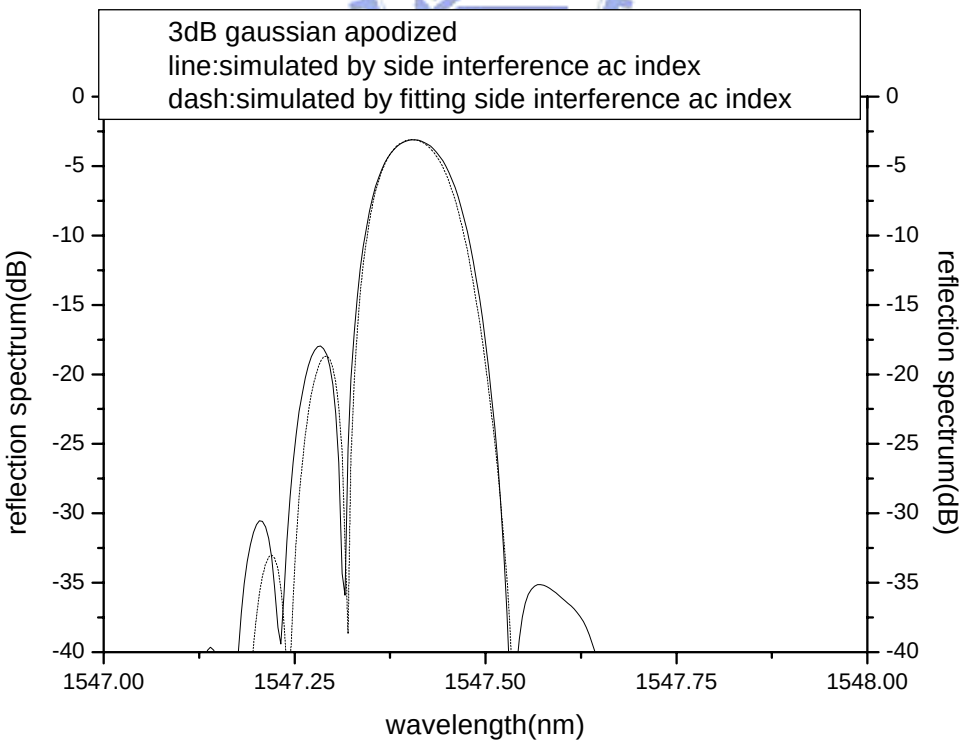

Fig.3.18 Simulated reflection spectra

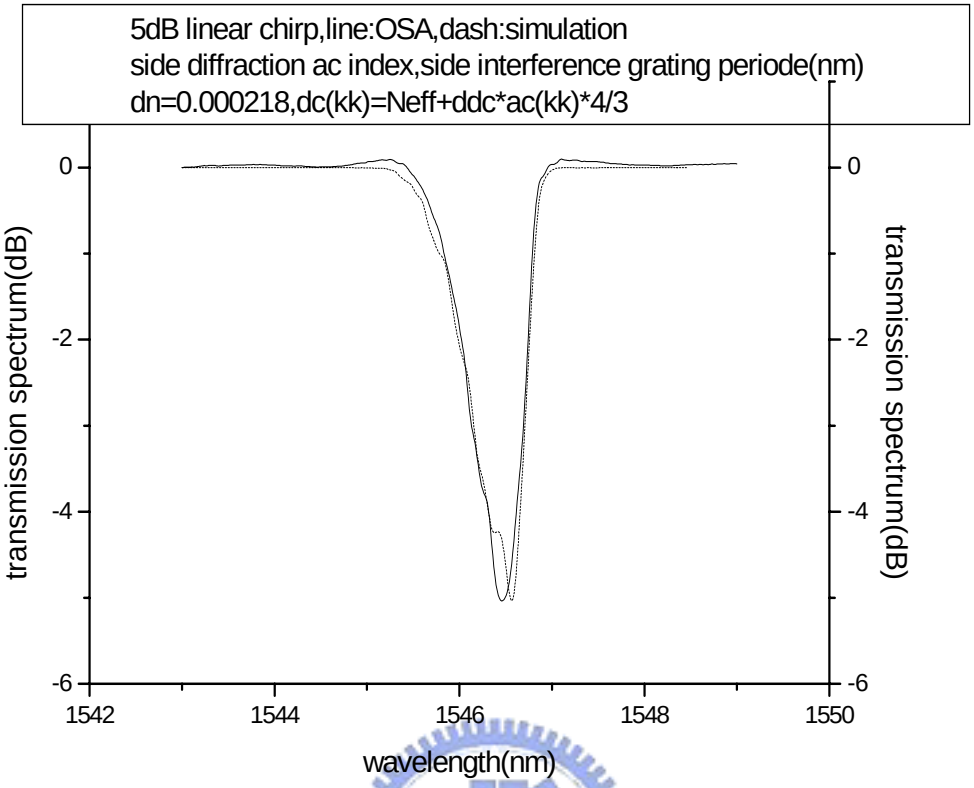

Fig.3.19 Transmission spectrum by simulation and by OSA

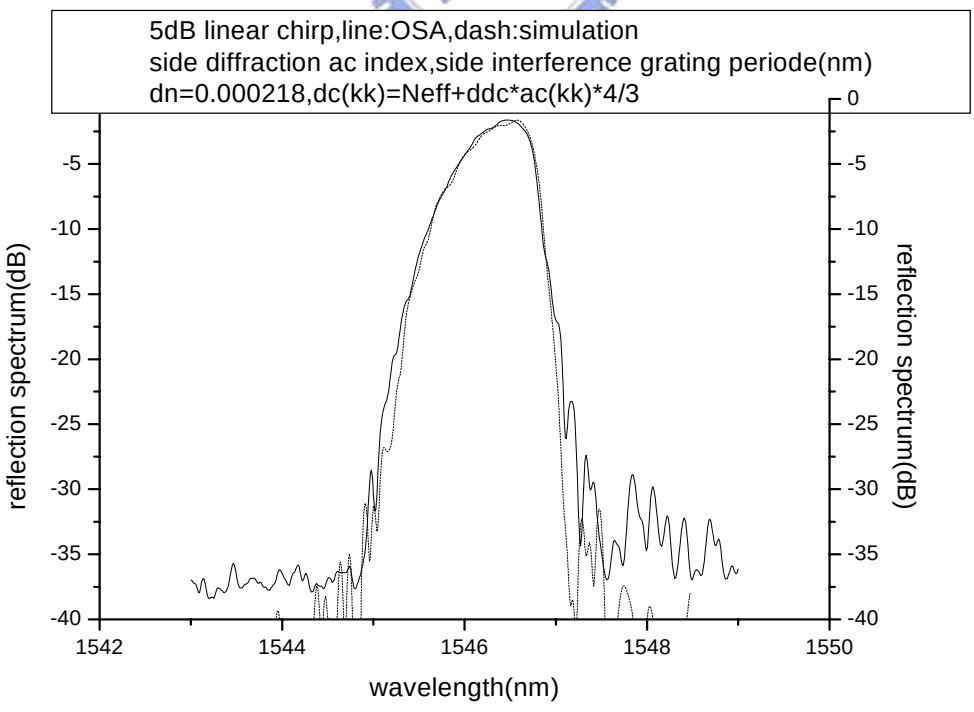

Fig.3.20 Reflection spectrum by simulation and OSA

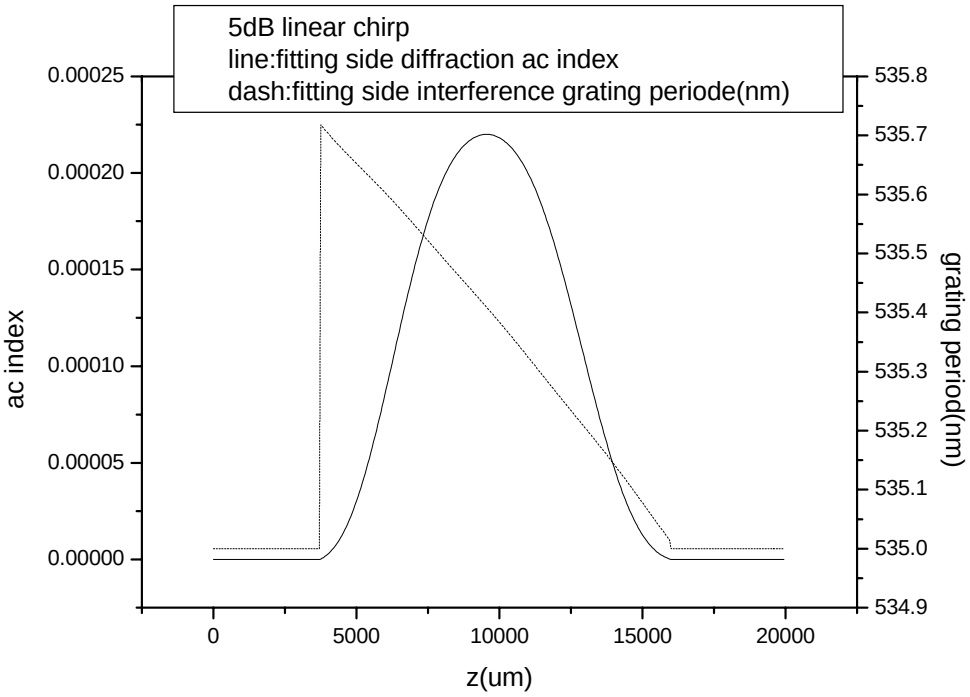

Fig.3.21 Fitting side diffraction ac index and fitting grating period

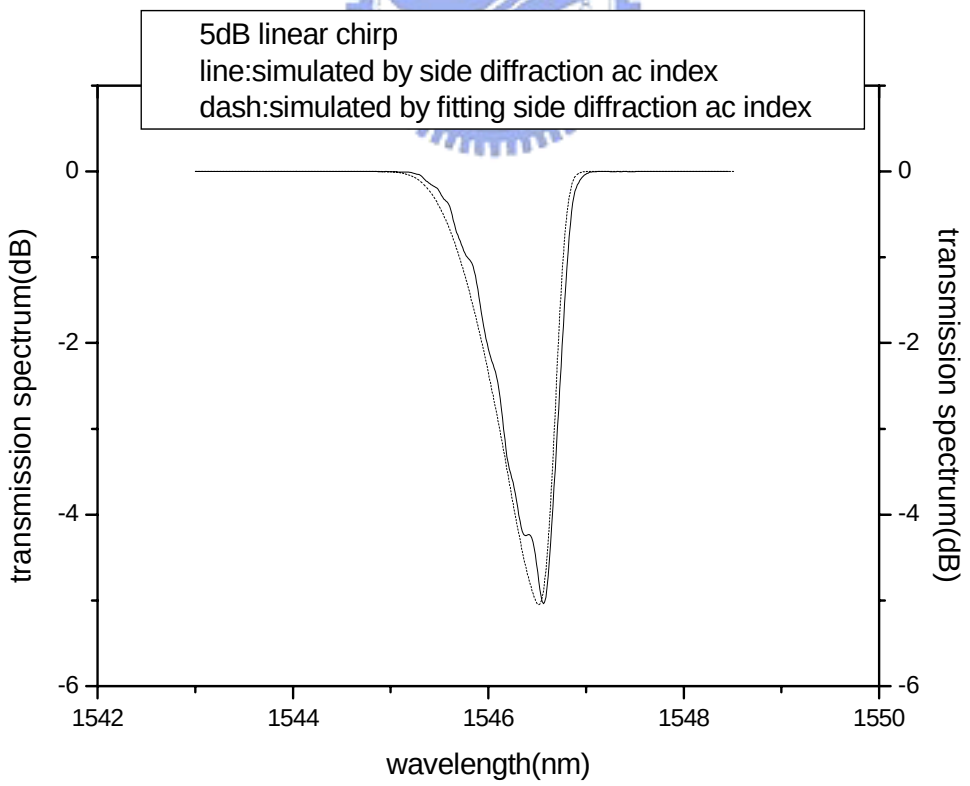

Fig.3.22 Simulated transmission spectra

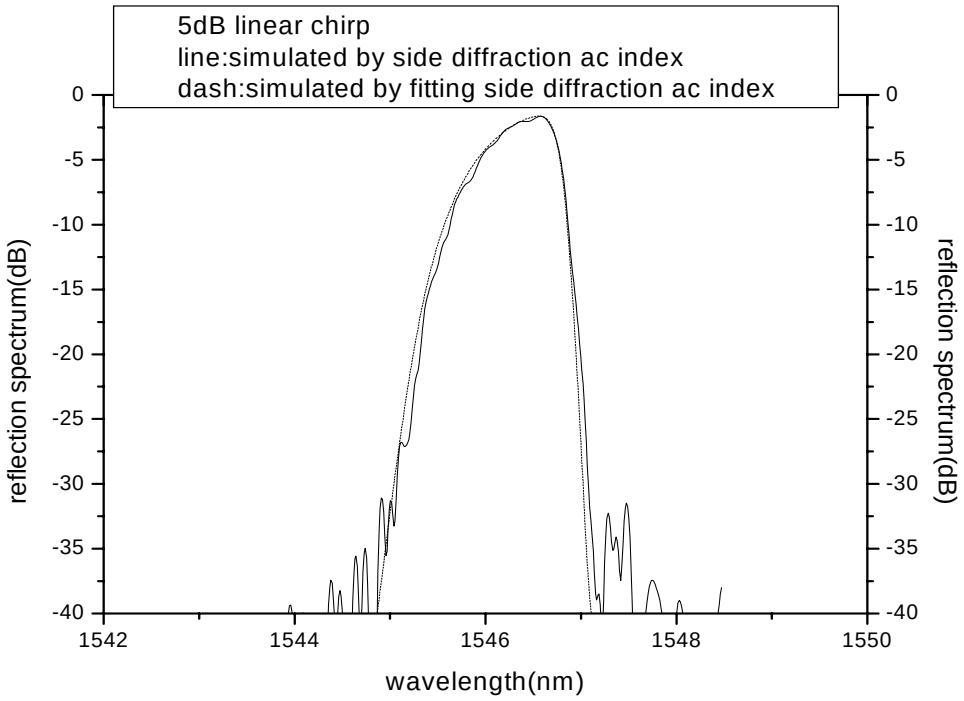

Fig.3.23 Simulated reflection spectra

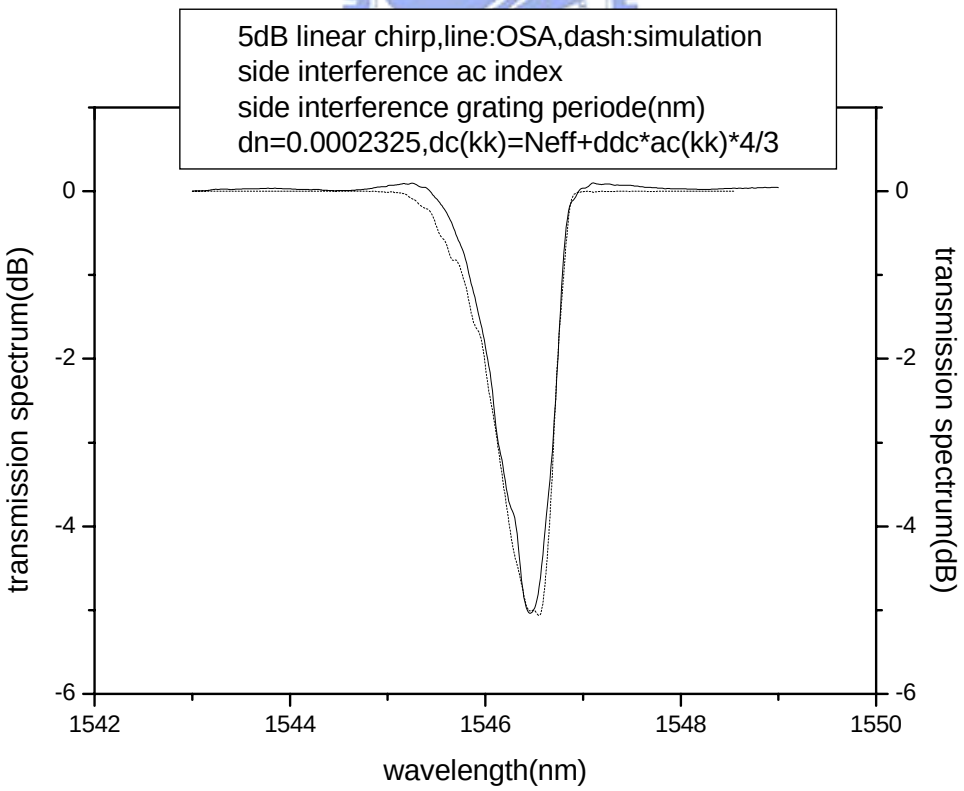

Fig.3.24 Transmission spectrum by simulation and by OSA

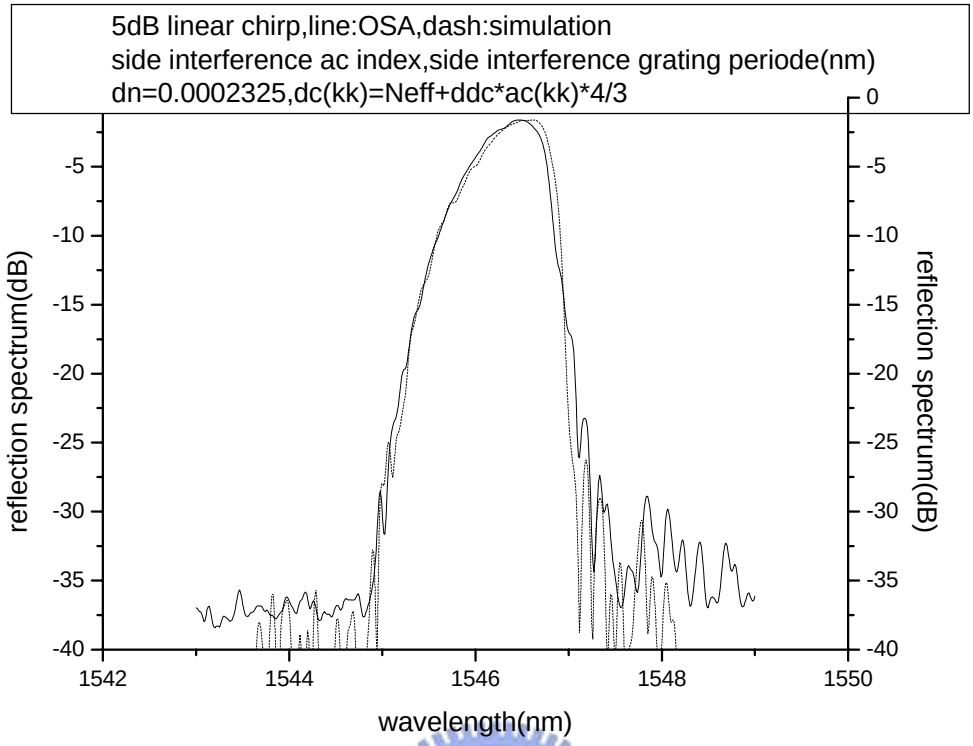

Fig.3.25 Reflection spectrum by simulation and OSA

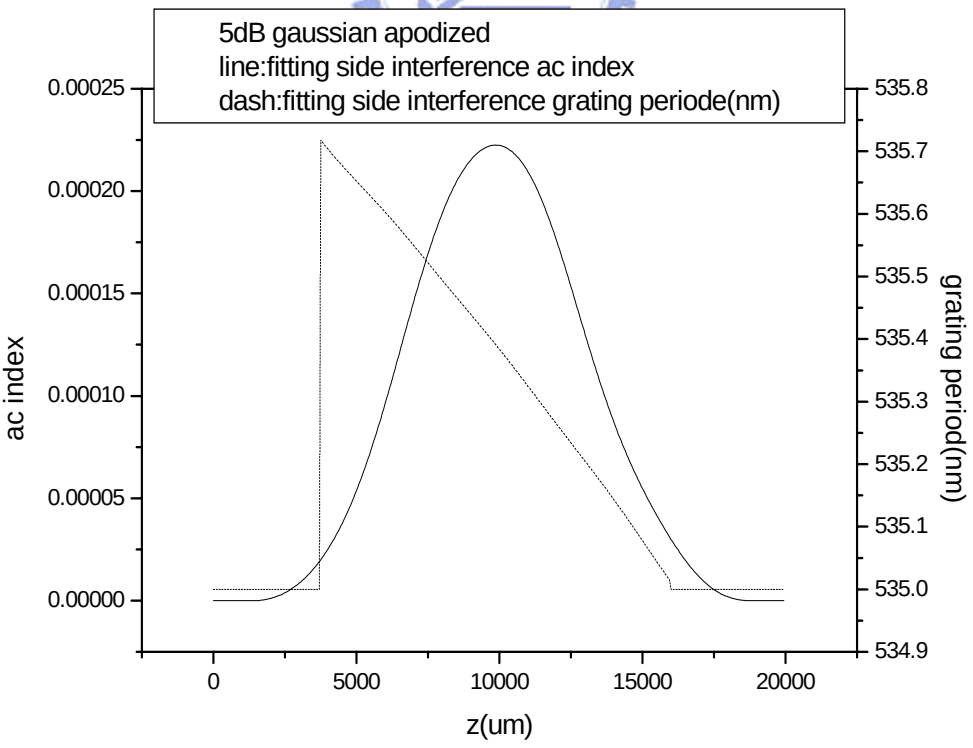

Fig.3.26 Fitting side interference ac index and fitting grating period

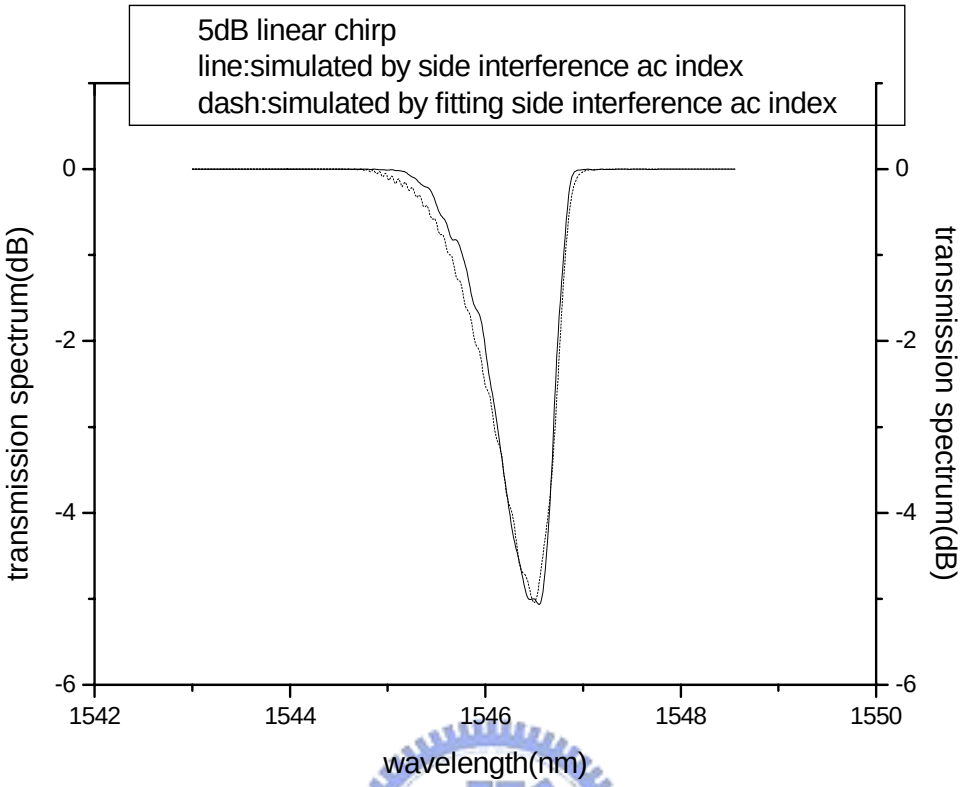

Fig.3.27 Simulated transmission spectra

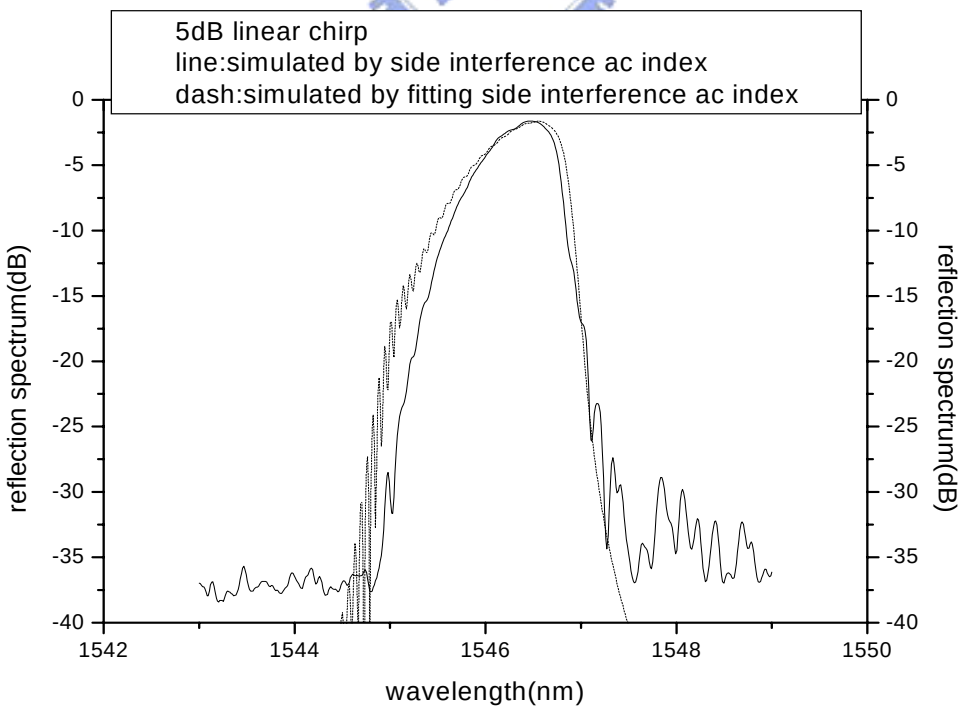

Fig.3.28 Simulated reflection spectra

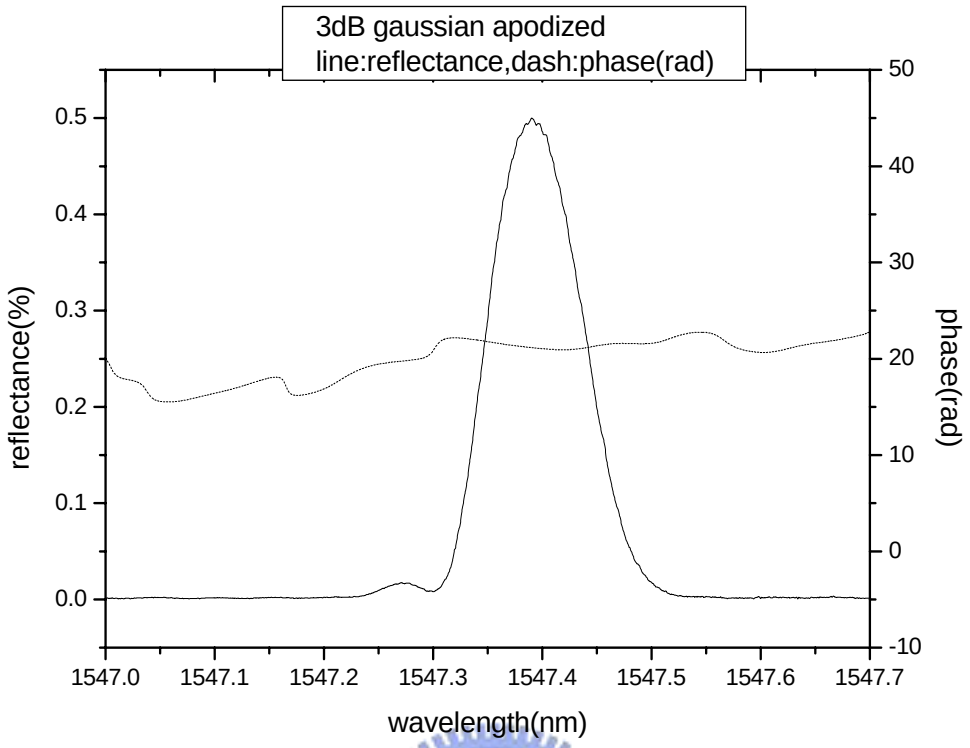

Fig.3.29 The phase of the 3dB Gaussian apodized grating

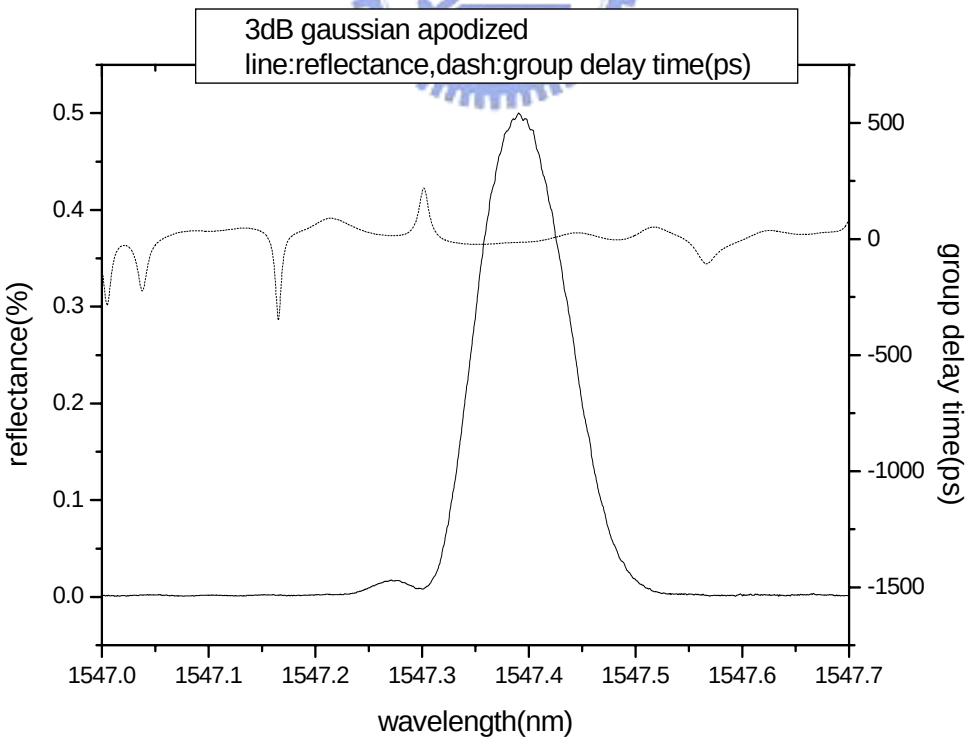

Fig.3.30 The group delay time of the 3dB Gaussian apodized grating

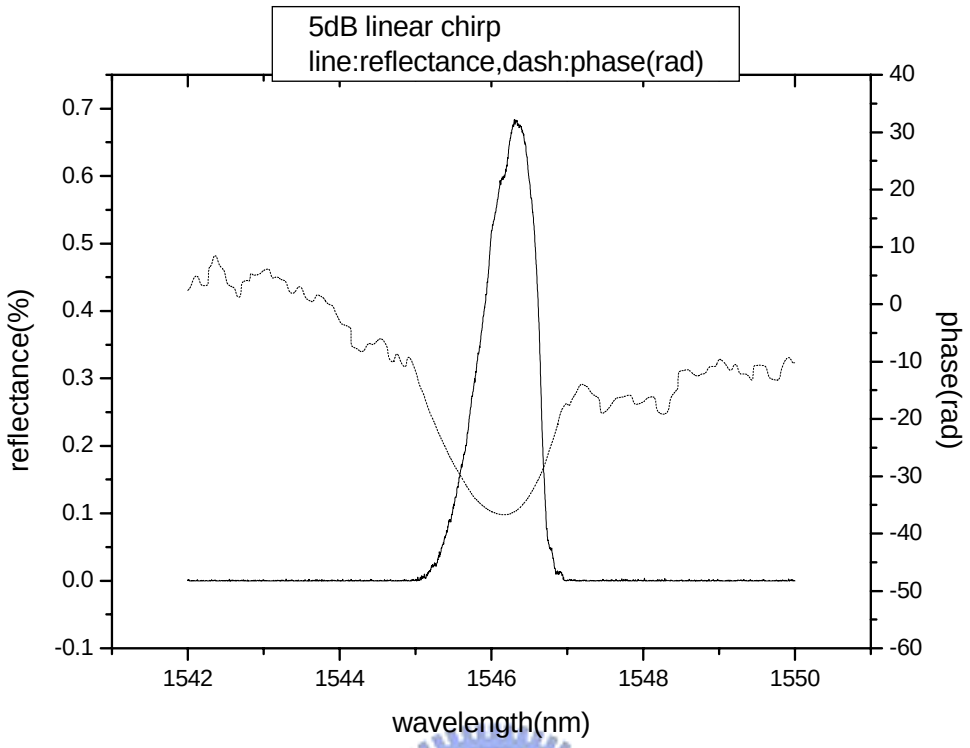

Fig.3.31 The phase of the 5dB linear chirp grating

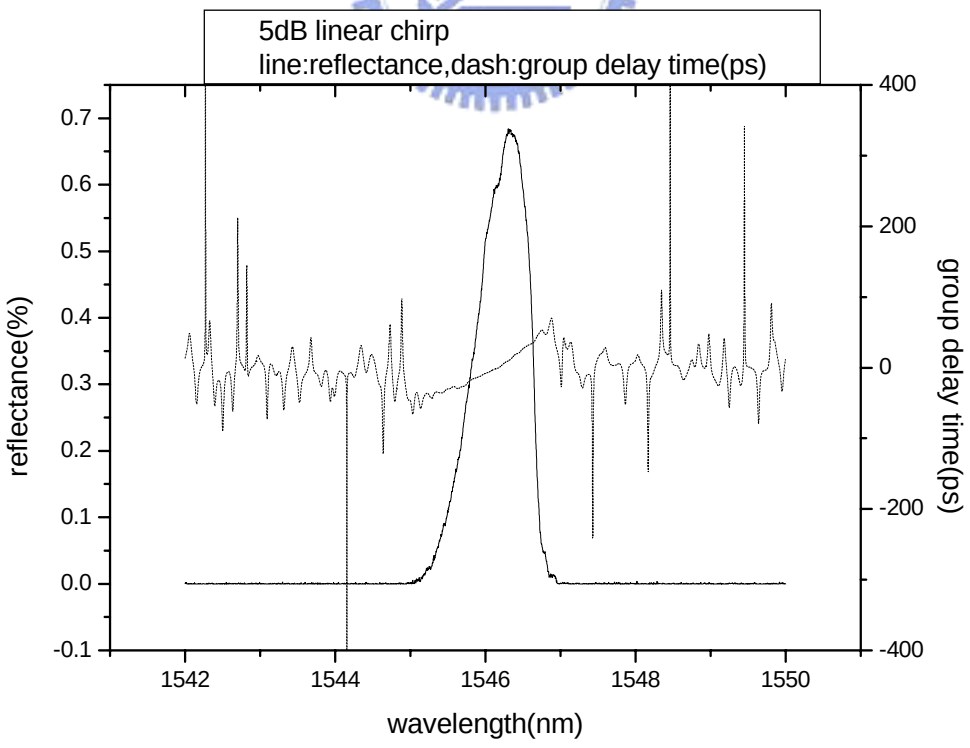

Fig3.32 The group delay time of the 5dB linear chirp grating

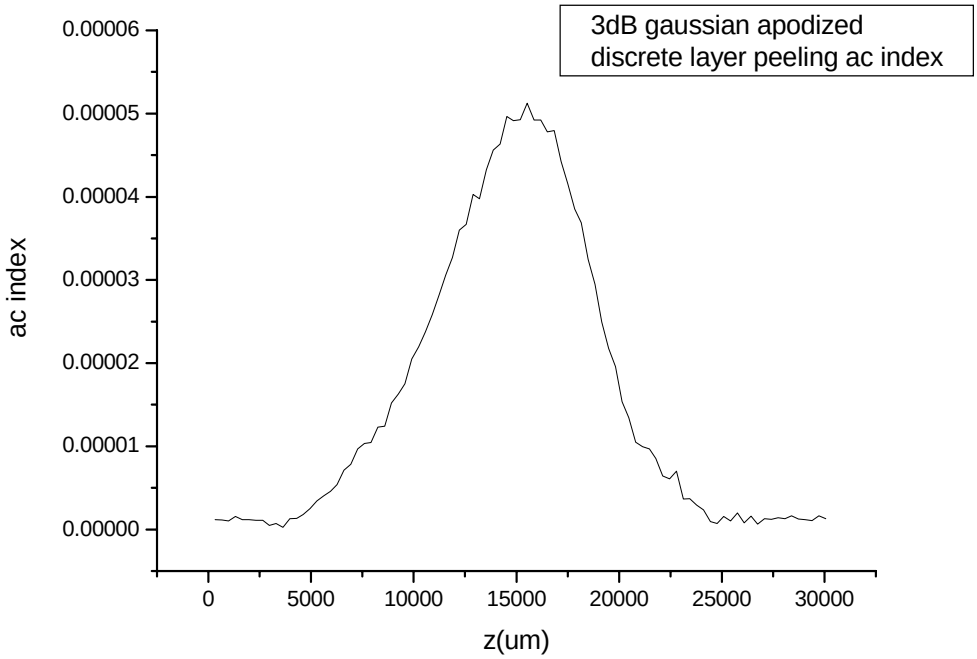

Fig.3.33 The ac index profile reconstructed by discrete layer peeling method

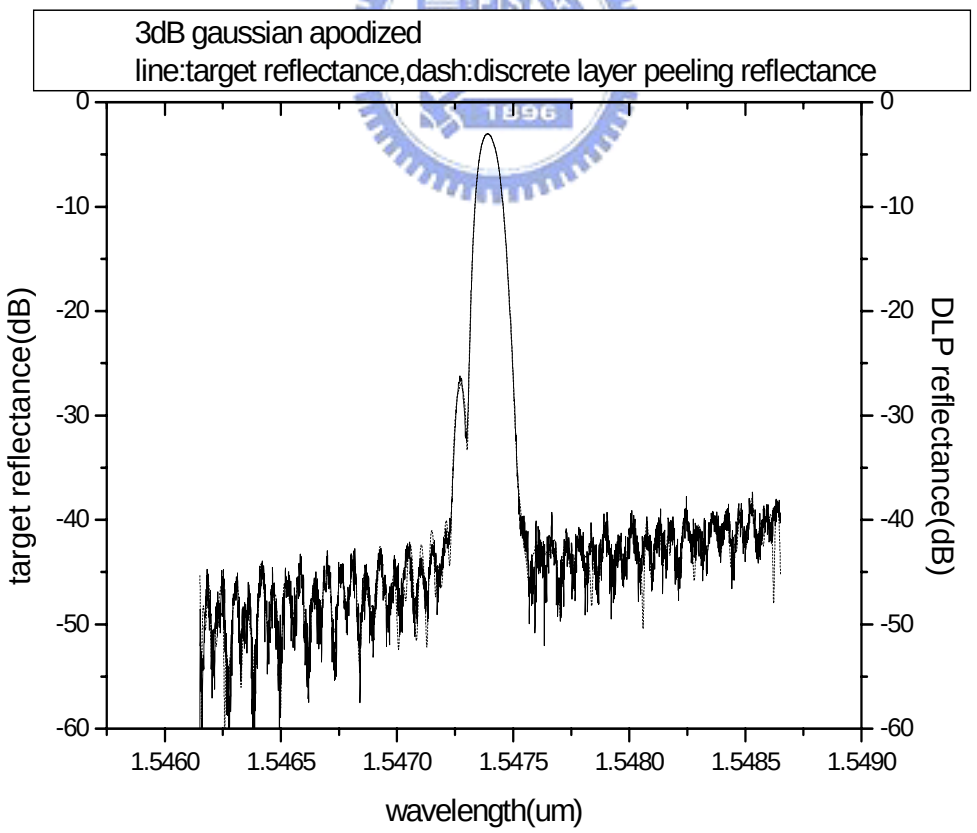

Fig.3.34 The target reflectance and reflectance simulated by DLP

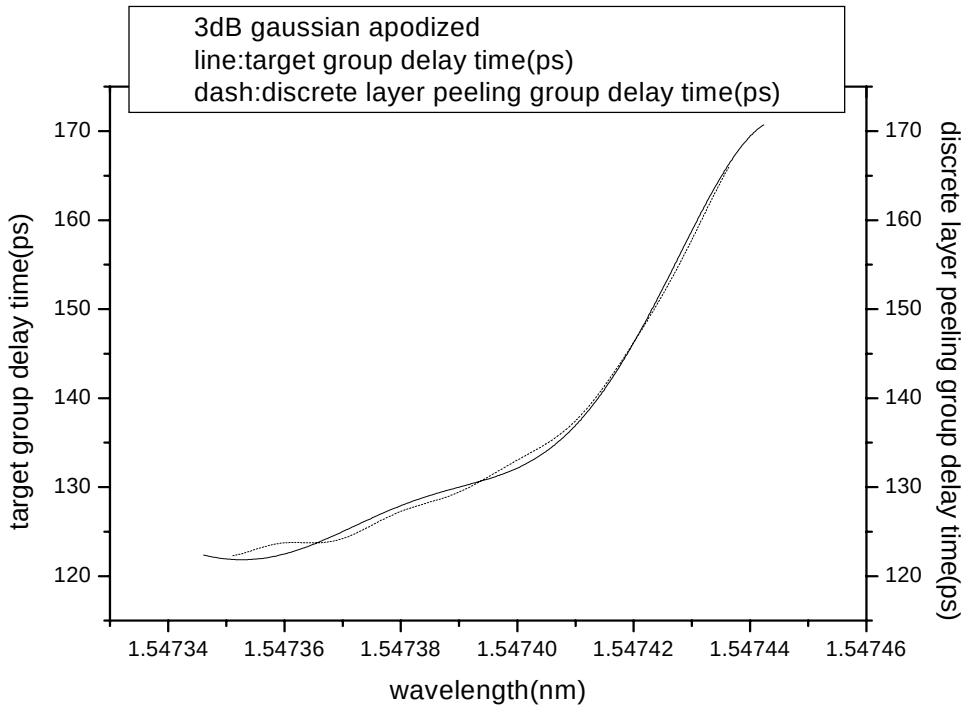

Fig.3.35 The target group delay time and group delay time simulated by DLP

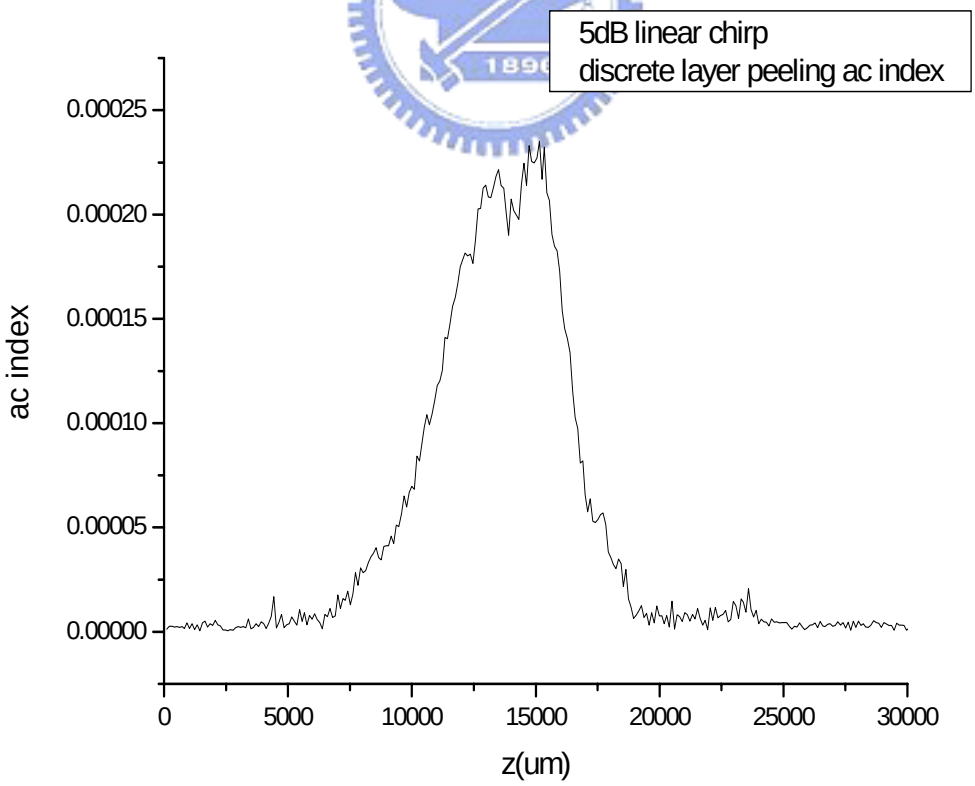

Fig.3.36 The ac index profile reconstructed by discrete layer peeling method

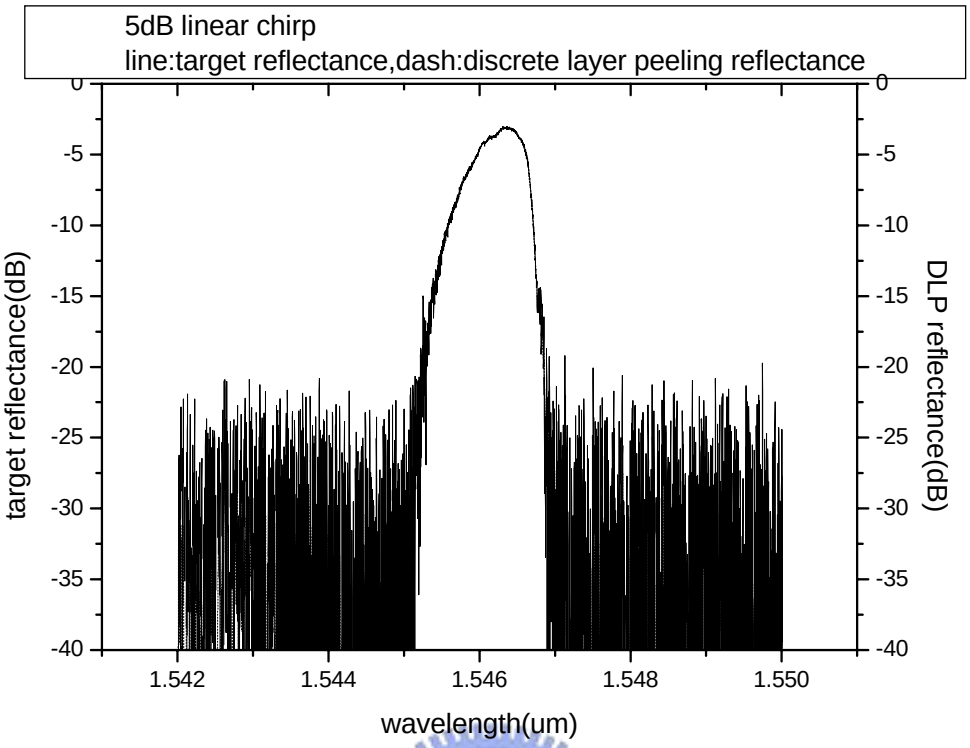

Fig.3.37 The target reflectance and reflectance simulated by DLP

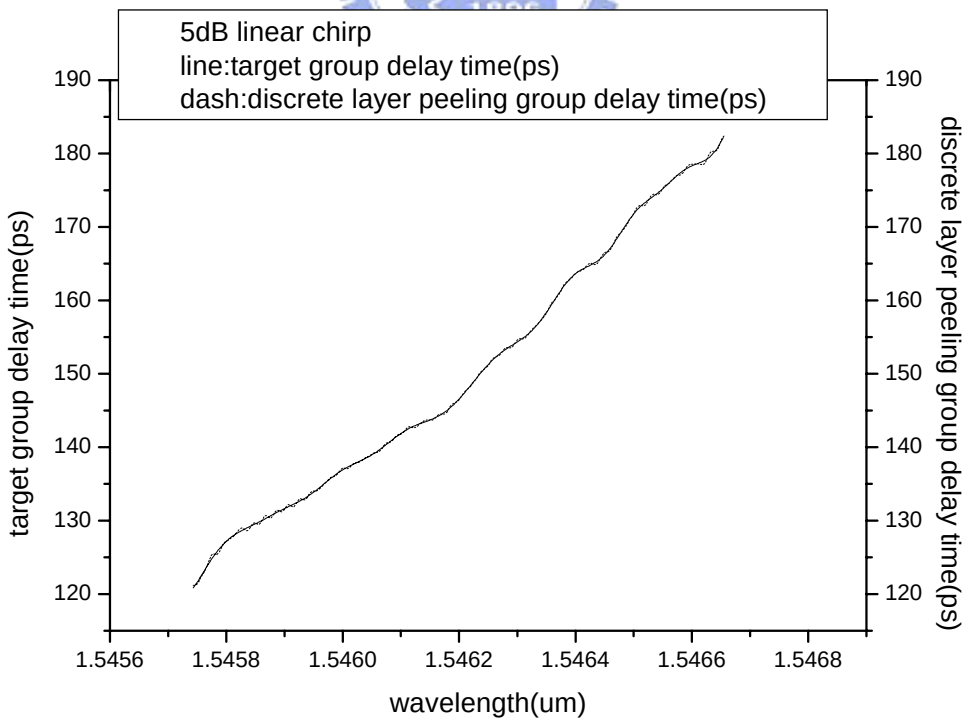

Fig.3.38 The target group delay time and group delay time simulated by DLP

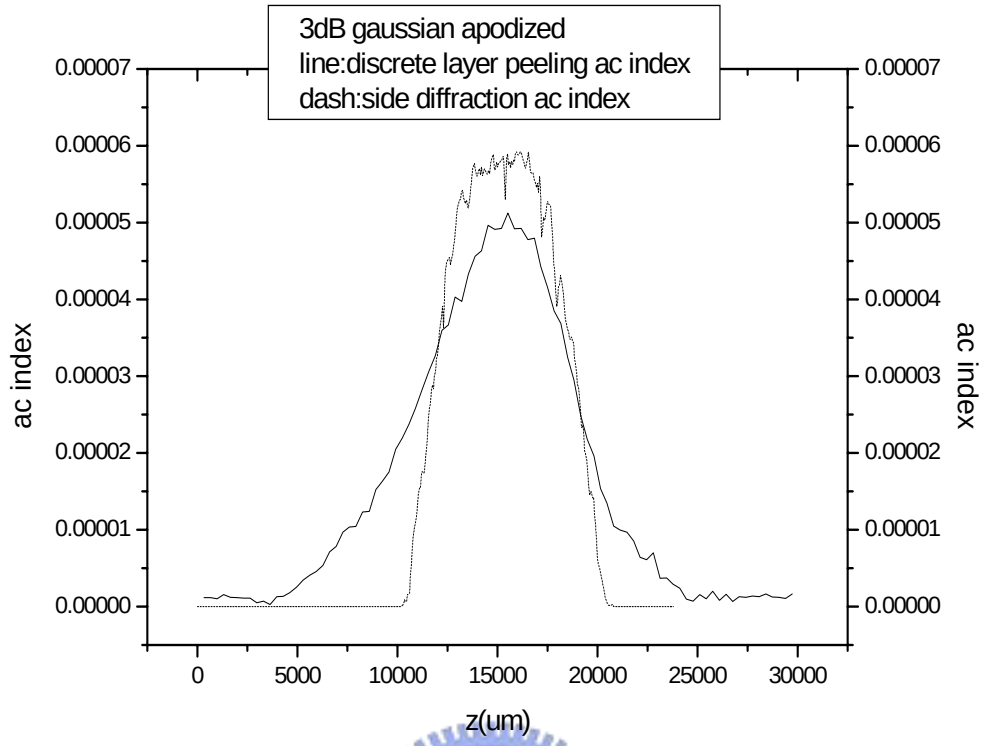

Fig.3.39 The ac index profile by side diffraction and discrete layer peeling

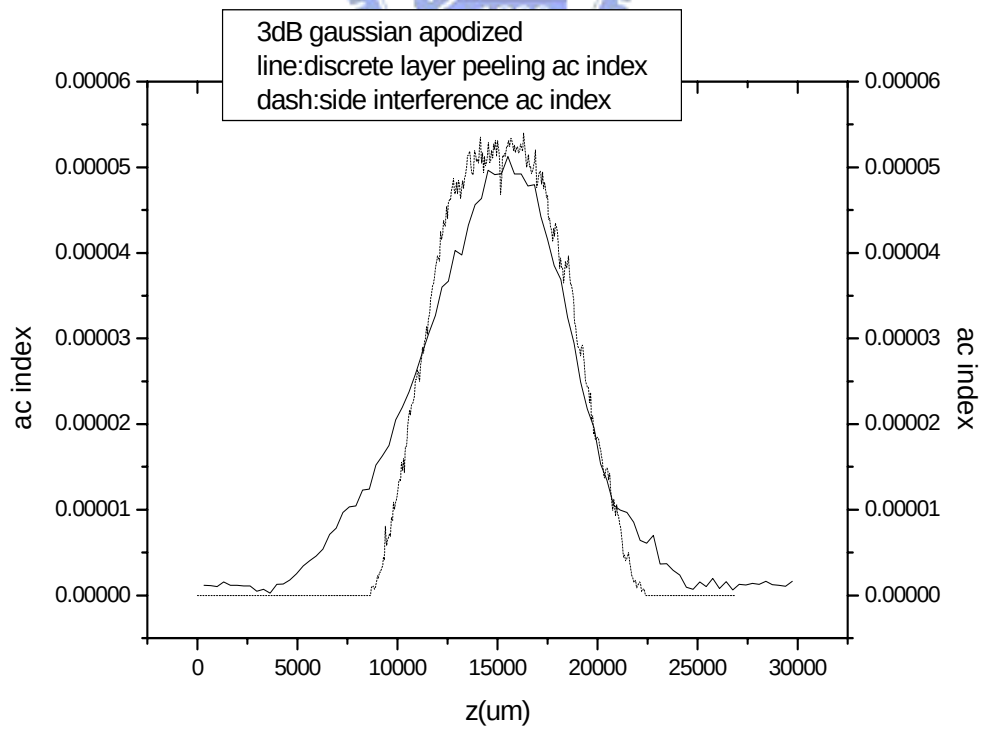

Fig.3.40 The ac index profile by side interference and discrete layer peeling

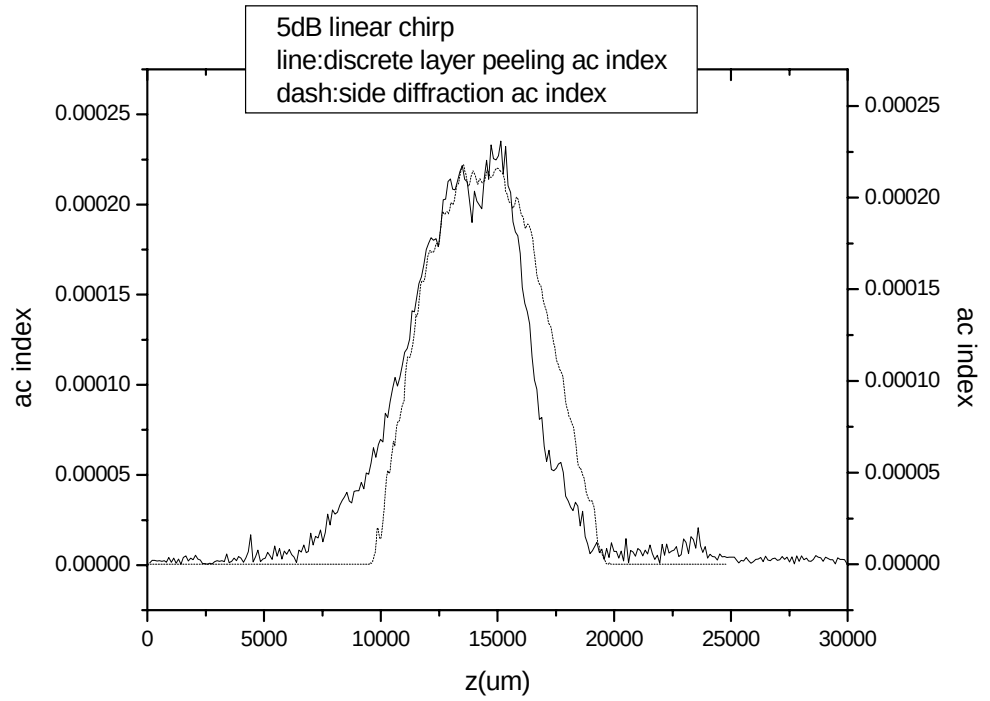

Fig.3.41 The ac index profile by side diffraction and discrete layer peeling

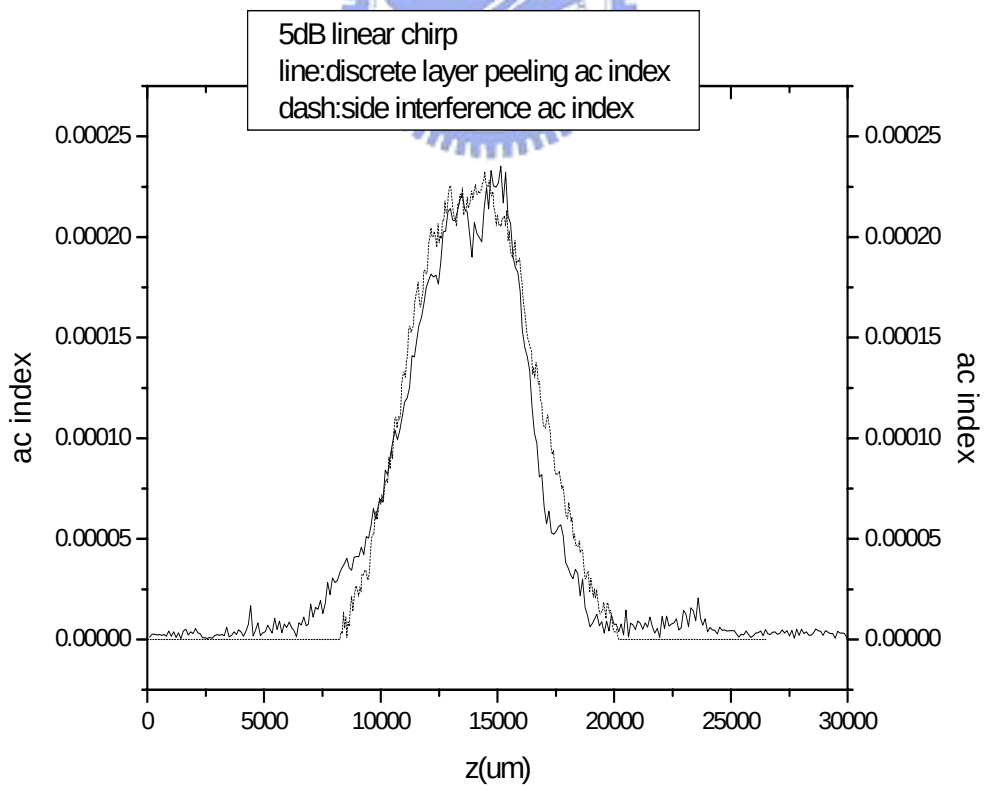

Fig.3.42 The ac index profile by side interference and discrete layer peeling

Chapter 4 Conclusions

We have demonstrated a direct method to measure the axial variation of the amplitude of the ac index modulation and the grating period of an optical fiber Bragg grating with a spatial resolution of approximately 80 μ m. This technique relies on the interference of a diffracted laser probe beam and a laser reference beam. Because the measured index change in the tails of the index profile is about $1*10^{-6}$, the demonstrated accuracy for measuring the ac index modulation is about $1*10^{-6}$, and the demonstrated accuracy for measuring the variation in the grating period is about 0.01nm. The axial ac modulation amplitude profile measured for the grating under test is in good agreement with the profile expected from the writing geometry, assuming that the UV writing mechanism is a single photon process. The variation of the grating period is also in agreement with the spec of the mask. The reflection and transmission spectra simulated by the transfer matrix method and the structure parameters above are in good agreement with those measured by the optical spectrum analyzer. In addition to the direct measurement of the structure parameters, we also perform an indirect method to reconstruct the axial variation of the amplitude of the ac index modulation. We use a Michelson interferometer to measure the phase shift and the group delay time of the fiber Bragg grating. Then by the use of the discrete layer peeling with the measured reflection intensity spectrum and phase spectrum, we can reconstruct the axial variation of the amplitude of the ac index modulation. The ac index profiles obtained by two methods are in good agreement. The direct side diffraction interference method lends itself to a real time monitoring techniques during the writing process. This method is also sensitive and is applicable even in the case of weak gratings with relatively low diffraction efficiency. Further more, there is negligible danger of fiber damage when this technique is used. Because the reflection

and transmission spectra simulated by raw ac profiles and fitting ac profiles are quite the same, we also confirm that the optical properties of many fiber Bragg grating devices are only affected by errors that occur over a relatively large (millimeter) length scale.

References

1. R. Kashyap, "***Fiber Bragg gratings***," Academic Press(1999)
2. A. Othonos, "Fiber Bragg gratings," Rev. Sci. Instrum. 68, 4309-4341(1997)
3. K. O. Hill, Y. Fujii, D. C. Johnson, and B. S. Kawasaki, "Photosensitivity in optical fiber waveguides: application to reflection fiber fabrication, Appl. Phys. Lett. 32, 647-649(1978)
4. K. O. Hill, B. Malo, F. Bilodeau, and D. C. Johnson, "Photosensitivity in optical fibers," Annu. Rev. Mater. Sci. 23, 125-157(1993)
5. W. W. Morey, G. A. Ball, and G. Meltz, "Photoinduced Bragg gratings in optical fibers," Opt. Photon. News 5, 8-14(1994)
6. G. Meltz, W. W. Morey, and W. H. Glenn, "Formation of Bragg gratings in optical fibers by transverse holographic method," Opt. Lett. 14, 823-825(1989)
7. Y. Rao, "In fiber Bragg grating sensors," Meas. Sci. Technol. 8, 355-375(1997)
8. D. Pastor, J. Capmany, D. Ortega, V. Tatay, and J. Marti, "Design of apodized linearly chirped fiber Bragg gratings for dispersion compensation," J. Lightwave Technol. 14, 2581-2588(1996)
9. B. J. Eggleton, P. A. Krug, L. Poladian, K. A. Ahmed. and H. F. Liu, "Experimental demonstration of compression of dispersed optical pulses by reflection from self chirped optical fiber Bragg gratings," Opt. Lett. 19, 877-879(1994)
10. T. Erdogan, "Fiber grating spectra," J. Lightwave Technol. 15, 1277-1294(1997)
11. K. Takada, I. Yokohama, K. Chida, and J. Noda, " New measurement system foe fault location in optical waveguide devices based on an interferometric technique," Appl. Opt. 26, 1603-1606(1987)
12. B. L. Danielson and C. D. Whittenberg, "Guided wave reflectometry with

micrometer resolution," Appl. Opt. 26, 2836-2842(1987)

13. P. Lambelet, P. Y. Fonjallaz, H. G. Limberger, R. P. Salathe, C. Zimmer, and H. H. Gilgen, "Bragg grating characterization by optical low coherence reflectometry," IEEE Photon. Technol. Lett. 5, 565-567(1993)
14. W. Margulis, I. G. Carvolho, and P. M. Gouvea, "Heat scan: a simple technique to study gratings in fiber," Opt. Lett. 18, 1016-1018(1993)
15. P. J. Lemaire, R. M. Atkins, V. Mizrahi, and W. A. Reeed, "High pressure H2 loading as a technique for achieving ultrahigh UV photosensitivity and thermal sensitivity in GeO2 doped optical fibers," Electron. Lett. 29, 1191-1193(1993)
16. R. Stubbe, B. Sahlgren, S. Sandgren, and A. Asseh, "Photosensitivity and Quadratic Nonlinearity in Glass Waveguides (Fundamentals and applications)," Postdeadline papers, Portland(1995)
17. A. Asseh, H. Storoy, B. E. Sahlgren, S. Sandgren, and R. Stubbe, "A writing technique for long fiber Bragg gratings with complex reflectivity profiles," J. Lightwave Tech. 15, 1419-1423(1997)
18. A. W. Snyder and J. D. Love, "Optical Waveguide Theory," Chapman & Hall (1983)
19. H. Kogelnik, "Filter response of nonuniform almost periodic structures," Bell Sys.Tech. J. 55, 109-126(1976)
20. D. Marcuse, "Theory of Dielectric Optical Waveguides," New York: Academic (1991)
21. L. Poladian, "Response Mode expansions and Exact Solutions for Nonuniform Greatings," Phys. Rev. E 54, 2963-2975(1996)
22. J. Skaar, " **Synthesis and characterization of fiber Bragg gratings**," (2000)
23. P. A. Krug, R. Stolte and R. Ulrich, "Measurement of index modulation along an

optical fiber Bragg grating," Optics Letters, Vol20, No17(1995)

24. L. M. Baskin, M. Sumetsky, P. S. Westbrook, P. I. Reyes, and B. J. Eggleton, "Accurate Characterization of Fiber Bragg Grating Index Modulation by Side diffraction Technique," IEEE photonics technology letters, Vol 15, No 3, March (2003)
25. F. E. Diasty, A. Heaney, and T. Erdogan, "Analysis of fiber Bragg gratings by a side diffraction interference technique," Applied Optics, Vol 40, No 6, 20 February (2001)
26. M. C. Tsai, "Chromatic dispersion measurement and structure reconstruction of fiber Bragg gratings," master thesis, Ieo NCTU(2003)